www.sciencemag.org/cgi/content/full/science.1227079/DC1

Supplementary Materials for

Detecting Causality in Complex Ecosystems

George Sugihara,* Robert May, Hao Ye, Chih-hao Hsieh,* Ethan Deyle, Michael Fogarty, Stephan Munch

*To whom correspondence should be addressed. E-mail: gsugihara@ucsd.edu (G.S.); chsieh@ntu.edu.tw (C.-h.H.)

Published 20 September 2012 on *Science* Express
DOI: 10.1126/science.1227079

This PDF file includes:

Materials and Methods
Figs. S1 to S5
GC Calculations S1 to S5
Tables S1 to S26
Box S1
Legends for movies S1 to S3
References

Other Supplementary Material for this manuscript includes the following:

Movies S1 to S3

Materials and Methods

Box S1 gives a simple example that illustrates nonseparability, and provides an example of the conflict between GC and Takens' Theorem. It provides an algebraic illustration of Takens' Theorem.

Movies S1, S2 and **S3** are short animations that illustrate the SSR and dynamical systems concepts used in this paper.

Notation

Variable	Description
ϕ	The dynamic process (temporal flow) that "evolves" states in the system through time. ϕ occurs on some d-dimensional manifold $\boldsymbol{M}$ (e.g. an attractor).
$\underline{m}(t)$	The vector on M representing the state of the system at time t. If $\underline{m}(t)$ is a point on $\boldsymbol{M}$, and ϕ is the flow, then $\underline{m}(t+1) = \phi(\underline{m}(t))$.
$\boldsymbol{M}$	The manifold (attractor) comprised of all trajectories and possible states $\underline{x}(t)$ of the system. $\boldsymbol{M}$ is a d-dimensional manifold embedded in an E-dimensional state space ($d \leq E$). The state space contains the manifold and its dynamics and consists of the original E Cartesian coordinates (fundamental variables) of the system.
X	An observation function of the system (X is commonly thought of as a "variable" under ϕ). X may correspond to a Cartesian coordinate of the actual E-dimensional state space containing $\boldsymbol{M}$, but more generally is a function (e.g. rotations or linear combinations of the original E Cartesian coordinates) that maps points in $\boldsymbol{M}$ to an observation (i.e. X: $\boldsymbol{M} \rightarrow \mathbb{R}$).
$\{X\}$	The time series corresponding to the values of variable X evolving through time. Thus, $\{X\}$ can be thought of as a serial projection of dynamics occurring on some manifold $\boldsymbol{M}$ onto a specific coordinate axis, X, recording displacements along that dimension through time.
$\boldsymbol{M_X}$	The shadow manifold reconstructed using time lags of $\{X\}$.
$\underline{x}(t)$	The vector on $\boldsymbol{M_X}$ corresponding to the state of the system at time t.
ϕ_X	The representation of the dynamic process ϕ, but occurring for points on the reconstructed shadow manifold $\boldsymbol{M_X}$.
$\hat{Y}(t) \mid \boldsymbol{M_X}$	The estimate of variable Y obtained by cross mapping using a shadow manifold $\boldsymbol{M_X}$ created from lags of $\{X\}$ (Fig. 2, Fig. S1).

Background definitions for causation in dynamic systems

Here we present a formal exposition of the criterion for causality presented in this work. The ideas are built from the theory of time-delay embedding first noted by Crutchfield (*35*), and later proven by Takens (*19*), then subsequently generalized (*20, 36*).

Consider a dynamic process ϕ defining the temporal evolution of points in an E-dimensional state space, trajectories of which converge to some d-dimensional ($d \leq E$) manifold $\boldsymbol{M}$ such that ϕ: $\boldsymbol{M} \rightarrow \boldsymbol{M}$. That is, if $\underline{m}(t)$ is a point on $\boldsymbol{M}$ then $\underline{m}(t+1) = \phi(\underline{m}(t))$.

Let X be an observation function of ϕ. X is commonly thought of as a system variable, but more generally is a function (e.g. rotation or linear combination of the original E coordinates) that maps points in $\boldsymbol{M}$ to a real-valued scalar (i.e. X: $\boldsymbol{M} \rightarrow \mathbb{R}$). For each X there is a

corresponding time series, $\{X\} = \{X(1), ..., X(L)\}$, that tracks the trajectory of points in $\boldsymbol{M}$ mapped to a sequence of real numbers, that is $X(t+1) = X(\underline{m}(t))$. The length of the time segment (library size) is L.

A lagged-coordinate embedding uses E time-lagged values of $\{X\}$ as coordinate axes or dimensions to reconstruct a shadow attractor manifold $\boldsymbol{M_X}$ (*3, 8, 19, 20, 24, 35, 37-40*). The points in this manifold, denoted by $\underline{x}(t)$, consist of the set of E-dimensional vectors: $\underline{x}(t) = \langle X(t), X(t-\tau), X(t-2\tau), ..., X(t-(E-1)\tau)\rangle$ where the time lag τ is positive. Generically, points $\underline{x}(t)$ on $\boldsymbol{M_X}$ map 1:1 to points $\underline{m}(t)$ on $\boldsymbol{M}$ (*19, 20*) so that $\boldsymbol{M_X}$ is a diffeomorphic reconstruction of the original attractor manifold $\boldsymbol{M}$ (*19, 20*). We note that there are special cases (discussed below) where the mapping between manifolds is asymmetrical and not 1:1.

The validity of an embedding can be confirmed if the manifold $\boldsymbol{M_X}$ constructed from historical time series values (a subset of $\{X\}$) can skillfully forecast points in an out-of-sample complement. This tests whether the attractor is sufficiently unfolded so that trajectories do not cross (no singularities). A manifold $\boldsymbol{M_X}$ constructed from lagged-coordinate vectors of X captures the dynamics of X when out-of-sample predictability is significant (measured by an error statistic: MAE, RMSE, or the correlation between observed and predicted values, ρ) (*3, 8, 40*). Systems that are fully deterministic with time series observations that are noise-free will converge toward perfect predictability as L goes to infinity (i.e. MAE ~ 0 and $\rho \sim 1$). In practical application, $\boldsymbol{M_X}$ is an approximation that will display convergence up to the level set by observational error, process noise, and data length.

There are special cases that do not satisfy the requirements for manifold reconstruction (*20*). For example, in the canonical Lorenz attractor, the coordinate Z does not produce a valid shadow manifold. Because the lobes of the attractor are symmetric with respect to Z and the two fixed points of the attractor (the center of the two lobes) have the same value for Z, the shadow manifold $\boldsymbol{M_Z}$ contains only a single fixed point, making it impossible to reproduce the full dynamics of the Lorenz system. However, if even a small rotation is made (e.g. if 0.01 X is added to Z), the new $\boldsymbol{M_Z}$ will be diffeomorphic with $\boldsymbol{M}$.

Convergent Cross Mapping (CCM)

A generic property of lagged-coordinate embedding is that points $\underline{x}(t)$ on $\boldsymbol{M_X}$ map 1:1 to points $\underline{m}(t)$ on $\boldsymbol{M}$ and local neighborhoods on $\boldsymbol{M_X}$ map to local neighborhoods on $\boldsymbol{M}$ (*19, 20*). It follows that for two variables X and Y that are dynamically coupled**,** local neighborhoods on their respective lagged reconstructions, $\boldsymbol{M_X}$ and $\boldsymbol{M_Y}$, will map to each other (*3, 8, 19, 20, 24, 27, 35, 37-42*) since X and Y are essentially alternative observations of the common attractor manifold $\boldsymbol{M}$ (Fig. S1A). Convergent cross mapping determines how well local neighborhoods on $\boldsymbol{M_X}$ correspond to local neighborhoods on $\boldsymbol{M_Y}$. To do so, a manifold $\boldsymbol{M_X}$ is constructed from lags of variable X and used to estimate contemporaneous values of Y. Because $\boldsymbol{M_X}$ is diffeomorphic to $\boldsymbol{M}$, estimates of Y converge as L goes to infinity (Fig. S2). In practical application, $\boldsymbol{M_X}$ is an approximation that will display convergence up to the level set by observational error and process noise. CCM is therefore demonstrated by estimation precision (or correlation) that rises with L and reaches a plateau.

An algorithm for CCM

Our algorithm for convergent cross mapping is based on simplex projection (*3*). Simplex projection is a nearest-neighbor algorithm that involves exponentially weighted distances from nearby points on a reconstructed manifold to do kernel density estimation (*19*).

Consider two time series of length L, $\{X\} = \{X(1), X(2), \ldots, X(L)\}$ and $\{Y\} = \{Y(1), Y(2), \ldots, Y(L)\}$. We begin by forming the lagged-coordinate vectors $\underline{x}(t) = \langle X(t), X(t\text{-}\tau), X(t\text{-}2\tau), \ldots, X(t\text{-}(E\text{-}1)\tau)\rangle$ for $t = 1+(E\text{-}1)\tau$ to $t = L$. This set of vectors is the "reconstructed manifold" or "shadow manifold" $\boldsymbol{M_X}$. To generate a cross-mapped estimate of $Y(t)$, denoted by $\hat{Y}(t) \mid \boldsymbol{M_X}$, we begin by locating the contemporaneous lagged-coordinate vector on $\boldsymbol{M_X}$, $\underline{x}(t)$, and find its E+1 nearest neighbors. Note that E+1 is the minimum number of points needed for a bounding simplex in an E-dimensional space (*3*). Next, denote the time indices (from closest to farthest) of the E+1 nearest neighbors of $\underline{x}(t)$ by $t_1, \ldots t_{E+1}$. These time indices corresponding to nearest neighbors to $\underline{x}(t)$ on $\boldsymbol{M_X}$ are used to identify points (neighbors) in Y (a putative neighborhood) to estimate $Y(t)$ from a locally weighted mean of the E+1 $Y(t_i)$ values.

$$\hat{Y}(t) \mid \boldsymbol{M_X} = \sum w_i \, Y(t_i) \qquad i = 1 \ldots E+1 \tag{S1}$$

where w_i is a weighting based on the distance between $\underline{x}(t)$ and its ith nearest neighbor on $\boldsymbol{M_X}$ and $Y(t_i)$ are the contemporaneous values of Y. The weights are determined by

$$w_i = u_i \Big/ \sum u_j \qquad j=1 \ldots E+1 \tag{S2}$$

where

$$u_i = \exp\{-d[\underline{x}(t), \underline{x}(t_i)] \Big/ d[\underline{x}(t), \underline{x}(t_1)]\} \tag{S3}$$

and $d[\underline{x}(s), \underline{x}(t)]$ is the Euclidean distance between two vectors. Cross mapping from Y to X is defined analogously.

If X and Y are dynamically coupled, the nearest neighbors of $\boldsymbol{M_X}$ should identify the time indices of corresponding nearest neighbors on $\boldsymbol{M_Y}$. As L increases, the attractor manifold fills in and the distances among the E+1 nearest neighbors shrinks. Consequently, $\hat{Y}(t) \mid \boldsymbol{M_X}$ should converge to $Y(t)$ and $\hat{X}(t) \mid \boldsymbol{M_Y}$ should converge to $X(t)$. In this way, we use convergence of the nearest neighbors to test whether there is a correspondence between *states* on $\boldsymbol{M_X}$ and *states* on $\boldsymbol{M_Y}$.

<u>Directional coupling</u>

Bidirectional causality implies CCM in both directions, i.e. $\boldsymbol{M_X}$ cross maps Y and $\boldsymbol{M_Y}$ cross maps X (Fig. 3 and Fig. S1A). This is the generic 1:1 case discussed by Takens (*19*). Note that as the causative influence of X on the dynamics of Y increases, more information about the dynamics of X is encoded in the manifold $\boldsymbol{M_Y}$ constructed from a fixed number of observations of Y. Conversely, consider a variable X whose dynamics are insensitive to the state of Y, but the reverse is not true. This could occur, for example, if variable X corresponds to external forcing (Fig. S1B).

In this case, $\boldsymbol{M_Y}$ is a valid manifold that is diffeomorphic to the original manifold $\boldsymbol{M}$ and we expect convergent cross mapping of variable X using $\boldsymbol{M_Y}$. However, this special case does not have a 1:1 mapping between the reconstructed manifold $\boldsymbol{M_X}$ and $\boldsymbol{M}$, because the forcing variable X contains no information about the dynamics of Y. Therefore cross mapping of variable Y using $\boldsymbol{M_X}$ will not converge in the limit as L approaches infinity.

It is possible that there may be significant predictability for Y using $\boldsymbol{M_X}$ that depends on the conditional probability, $\Pr[Y(t) \mid X(t), X(t\text{-}\tau), ..., X(t\text{-}(E\text{-}1)\tau)]$. However, this predictability using $\boldsymbol{M_X}$ is not convergent (Fig. 4B). Cross mapping that converges in only one direction is the criterion for unidirectional causality. Moreover, because the cross mapping of Y using X does not converge, this indicates that there is incomplete information flow from Y to X, so that Y is not causal to X.

Note that this work focuses on the typical case where the intrinsic dynamics of the forced variable remain significant so that dynamics of the forced variable reflect more than just the driving system. Here, the complete manifold can be thought of as including both the driving system and the forced variable, and the driving system in turn can be thought of as operating on a lower dimensional sub-manifold of the complete system. However, it is possible to collapse the complete manifold to the sub-manifold when the intrinsic dynamics of the forced variable become "enslaved" by the driving subsystem. This can happen with pathologically strong forcing so that the dependence of the dynamics of the forced variable on its own state is no longer significant. This describes the well-known phenomenon of "synchronization" (*27*). Here the complete system collapses to the driving system sub-manifold, and the forced variable effectively becomes an observation function on the driving system. Here, unlike the case of asymmetric coupling above, Takens' theorem will apply, so that convergent cross mapping operates in both directions, as both variables are sensitive to the dynamics of the whole system. This pathological special case is difficult to distinguish from the bidirectional case.

Comment on time series length

In general, state space reconstruction (SSR) methods work best when the system is nonlinear and can be approximated in few dimensions, and especially when observational noise is not excessive. Although there are many published examples of applications of SSR in ecology, how broadly CCM applies remains to be seen. Nonetheless, it is encouraging that it works with time series data as sparse and noisy and potentially complex as those from fisheries. As Ruelle (*43*) noted, for reconstructions intended for attractor dimensions estimates, the amount of data required depends on the attractor dimensionality, with the resolution of the attractor varying roughly as the inverse power of its dimension. (Note that CCM is more concerned with the 'embedding dimension' (E), than the attractor dimension (d), but these are related by the Whitney embedding theorem ($E \leq 2d+1$)).

Although we cannot predict how broadly applicable the methods will be, for fisheries (at the NOAA/NMFS NLTS workshop held this spring (2012) at Scripps Institution of Oceanography investigating nonlinear time series methods), the SIO-WHOI CAMEO group found these methods effective in the majority of fisheries cases studied (~72 species) where the data are noisy and the time series are short (35-40 points). Hsieh et al. (*8*) found related state space reconstruction methods effective in a broad survey of marine biological time series of similar limited length for the 20th century.

Simulations and data sets

Here we provide details of the data sets analyzed in the main text. Section a) provides complete specification of the model examples, b) provides details on the *Paramecium-Didinium* time series and analysis, and c) provides details on the Sardine-Anchovy-Temperature data.

a) Description of the models

(i) Ephemeral regimes in a coupled dynamic system (Figure 1)

Figure 1 demonstrates the phenomenon of mirage correlation with three samples from a single run of a coupled 2-species nonlinear logistic difference system with constant coefficients: equation (1) with r_x =3.8, r_y = 3.5, $\beta_{x,y}$ = 0.02, $\beta_{y,x}$ = 0.1 and starting conditions $X(1) = 0.4$, $Y(1) = 0.2$.

(ii) General bidirectionally coupled dynamic system (Figure 2B)

The relative convergence rates for cross mapping are indicative of the interaction strength. Figure 2B summarizes this result for equation (1) using 1000 parameterizations with r and β chosen uniformly in the intervals [3.6, 4.0] and [0, 0.4] respectively. For each system, cross map estimates are computed for 1000 points using attractor reconstructions with $L = 400$ and $E = 2$.

(iii) Asymmetrically coupled dynamic system (Figures 2C-D)

Figures 2C-D demonstrate the usage of CCM for identifying the direction of causative influence in an asymmetrically coupled dynamic system: equation (1) with $\beta_{x,y}$ = 0 (r_x =3.7, r_y = 3.7, $\beta_{y,x}$ = 0.32) and starting conditions $X(1) = 0.2$, $Y(1) = 0.4$. 1000 cross map estimates are plotted using attractor reconstructions with $L = 1000$ and $E = 2$.

(iv) Example 1: External forcing of non-coupled variables (Figure 3B)

We analyzed a standard fishery model system with two non-interacting populations that share common environmental forcing. The populations obey an extended Schaffer model that includes reproductive delay and adult survival. Recruitment (R) to adults (N) includes a white noise environmental variable, T.

$$\begin{aligned} R_x(t+1) &= X(t)[3.1\,(1 - X(t))]\exp(-0.3\,T) \\ R_y(t+1) &= Y(t)[2.9\,(1 - Y(t))]\exp(-0.36\,T) \\ X(t+1) &= 0.4\,X(t) + \max(R_x(t-3), 0) \\ Y(t+1) &= 0.35\,Y(t) + \max(R_y(t-3), 0) \end{aligned} \tag{S4}$$

We compared cross-correlation and cross mapping between populations $X(t)$ and $Y(t)$ for different time series lengths, L. For each value of L, cross map predictability or cross-correlation values were averaged over 500 randomly chosen segments of length L from an 8000-point time series. The same segment was then estimated using leave-one-out cross-validation for all cross-mapping calculations. An optimal embedding dimension of $E = 4$ was found from univariate SSR of X and Y.

(v) Example 2: 5-species model (Figure 3C)

The equations below provide the explicit system of equations for the model. CCM results are shown in panel (C) of Figure 4. Cross map skill is the correlation between observations and estimates for L= 300. A different time series segment of 300 points was used for the attractor reconstructions.

Subsystem Y_1, Y_2 and Y_3 is the forcing subsystem, that interacts unidirectionally with Y_4 and Y_5. Y_4 and Y_5 do not interact with each other and do not influence Y_1, Y_2 and Y_3.

$$
\begin{aligned}
Y_1(t+1) &= Y_1(t)\,[4 - 4\,Y_1(t) - 2\,Y_2(t) - 0.4\,Y_3(t)] \\
Y_2(t+1) &= Y_2(t)\,[3.1 - 0.31\,Y_1(t) - 3.1\,Y_2(t) - 0.93\,Y_3(t)] \\
Y_3(t+1) &= Y_3(t)\,[2.12 + 0.636\,Y_1(t) + 0.636\,Y_2(t) - 2.12\,Y_3(t)] \\
Y_4(t+1) &= Y_4(t)\,[3.8 - 0.111\,Y_1(t) - 0.011\,Y_2(t) + 0.131\,Y_3(t) - 3.8\,Y_4(t)] \\
Y_5(t+1) &= Y_5(t)\,[4.1 - 0.082\,Y_1(t) - 0.111\,Y_2(t) - 0.125\,Y_3(t) - 4.1Y_5(t)]
\end{aligned}
\tag{S5}
$$

b) Empirical test of causality for the Didinium-Paramecium system

We demonstrate the CCM procedure using experimental time series from the classical *Paramecium-Didinium* protozoan prey-predator system. Expanding on earlier work by Gause (*44*) and Luckinbill (*45*), Veilleux (*28*) identified conditions that produced sustained oscillations in predators (*Didinium nasutum*) and prey (*Paramecium aurelia).* This protocol involved populations maintained at 27°C at a pH of 6.7-6.8 in petri dishes containing 6mL of medium with Cerophyll concentration of 0.9 g/L and methyl cellulose of 3.5 g/L. Every two days, 50% of the medium was replaced. Initial densities of *Paramecium* and *Didinium* were 15 and 5 individuals/ml, respectively. Abundance measurements were taken every 12 hours by thoroughly mixing the container and counting the number of individuals in 8 samples of 0.1 mL. The mean of these 8 samples was used to determine the density with errors of < 3.5%. The data analyzed appear in Jost and Ellner (*46*) and can be found at *http://robjhyndman.com/tsdldata/data/veilleux.dat*.

The first 10 data points were removed to eliminate transient behavior in the initial period of the experiment. The time series were then normalized to unit mean and variance prior to analysis. The best embedding dimension was E=3. To account for the limited length of time series, leave-one-out cross validation was used for the CCM analysis (*47*). That is, to find the nearest neighbors of $\underline{x}(t)$ in $\boldsymbol{M_X}$, $\underline{x}(t)$ and all vectors containing coordinates of $\underline{x}(t)$ are first removed from $\boldsymbol{M_X}$ to keep the mappings out-of-sample. All cross map correlations are truncated at 0.

c) *Empirical test of causality for the California Current Sardine-Anchovy-SST system*

Sea surface temperature (SST) was measured at shore stations: Scripps Pier and Newport Pier (data available from: http://shorestation.ucsd.edu/active/index_active.html). Following Lasker and MacCall (*31*), monthly means were averaged to form yearly time series, and the final time series consisted of 3-year running averages for the SST.

California landings data for Pacific sardine (*Sardinops sagax*) and northern anchovy (*Engraulis mordax*) were taken from two sources:

1. (1928 – 2002) NOAA Southwest Fisheries Science Center (http://las.pfeg.noaa.gov:8080/las_fish1/servlets/dataset?catitem=2)
2. (2003 – 2006) California Department of Fish and Game (http://www.dfg.ca.gov/marine/landings05.asp)

Landings time series from 1928 to 2006 were constructed for sardine and anchovy. Following Hsieh et al. (*8*), the data were first-differenced prior to analysis. CCM tested for linkages between sardine and anchovy, sardine versus Scripps Pier SST, and anchovy versus Newport Pier SST. An embedding dimension E = 3 was used for all CCM estimates. All cross map correlations are truncated at 0. To address the limited length of time series, leave-one-out cross validation was used for the analysis (*47*).

Supplementary Text

Alternative data tested for Sardine-Anchovy-SST CCM

The results given in Figure 4 of the main text are based on landings data. As a check, we examine the robustness of our analysis to stock abundance data for Pacific sardine and northern anchovy from other sources; namely the fishery independent CalCOFI ichthyoplankton surveys, and daily egg production data.

Yearly ichthyoplankton records (1951-2008) were constructed following Hsieh et al. (*48*), and have been shown to be a good indicator of adult spawning biomass (*49*). Because they are independent of the fishery, they eliminate potential confounding factors that could arise in landings data. Using identical methods as the previous analysis, CCM was used to test the relationship between sardine and anchovy, sardine versus Scripps Pier SST, and anchovy versus Newport Pier SST. Although there were sampling gaps in the ichthyoplankton time series (the surveys started in the 1950s and were only done triennially in 1966-1984) that were not present in the landings data, the CCM results remain similar (Fig. S3).

Daily egg production (DEP) data are a third proxy of adult biomass (*50*). We used CCM analysis to examine causality between DEP as a proxy for anchovy abundance, and SST. As can be seen in Figure S4, the CCM results clearly confirm that SST drives the anchovy population size and that anchovy DEP does not affect SST. Daily egg production data are not available for sardines in the California Current system.

Therefore, after repeating the CCM analysis on all available alternative data for the California Sardine-Anchovy-SST system, we find results that are consistent with the same causality network portrayed in Figure 5. On this basis we believe the result is robust. Thus, sea surface temperature is a common causal variable for California sardine and anchovy, but there is no causal interaction between these species, even though they can appear to be negatively correlated.

Alternative state-space reconstruction (SSR) techniques for detecting causality

There have been several attempts to infer causal relationships for nonseparable systems based on ideas of SSR (*41, 42, 51*); however, these have tended to focus on synchrony, and nearly all have assumed Granger's separability paradigm. In addition, none have considered the key property of convergence and none have provided effective criteria for detecting causality with weak to moderate coupling (or where observational noise is present). Schemes offered by both Arnhold et al. (*51*) and Le Van Quyen et al. (*42*) are both incorrect when inferring the direction of causation. Similarly, Marinazzo et al. (*52*) apply Granger's criterion to nonlinear systems using a kernel-based approach (that is similar to the Sugihara (*53*) S-map) to co-prediction. As with Granger, these authors assume that in a dynamic system where Y is influenced by X but not vice-versa, the time series $\{X\}$ will contain information about Y (at levels of coupling below synchrony). As shown throughout this work (and specifically, Box S1), this criterion should be reversed in general dynamic systems.

SSR methods involving embeddings constructed from trial and error searches over multiple time series are useful for system identification (finding key variables) (*4*). However they cannot distinguish correlated non-causal variables from true dynamic causation, and in similar vein, may not distinguish the direction of causation—particularly if they contain driving variables that are weak or even moderately strong.

Alone among SSR studies, Schiff et al. (*41*) make the correct directional inference about causation; however they fail to consider convergence, and their vector-based approach lacks skill

with weak to modest interaction strengths (particularly relevant for ecological systems). They illustrate this shortcoming in their Figure 3A (*41*) where their methods fail to detect causation in one-way coupled Henon maps. However, as shown in Table S1 below, CCM performs well with this example (using the same model as (*41*) with the exact parameters given in their Figure 3A).

Finally, all previous SSR-based methods fail to recognize the importance of convergence for identifying a manifold. Convergence is required to demonstrate causality, and failure to account for this has contributed to contradictory results in the literature.

To illustrate this, consider the coupled Rossler-Lorenz system discussed by Le Van Quyen et al. (*42*):

Rossler system:

$$\begin{aligned} dU/dt &= -\alpha\,(V + W) \\ dV/dt &= \alpha\,(U + 0.2\,V) \\ dW/dt &= \alpha\,(0.2 + W\,(U - 5.7) \end{aligned} \tag{S6}$$

Lorenz system:

$$\begin{aligned} dX/dt &= 10\,(-X + Y) \\ dY/dt &= 28\,X - Y - X\,Z + C\,V^2 \\ dZ/dt &= X\,Y - 8/3\,Z \end{aligned} \tag{S7}$$

where C is the strength of the unidirectional coupling between the two attractors and α controls the characteristic timescale of the driving system.

Without considering convergence, Le Van Quyen et al. (*42*) incorrectly found stronger cross prediction of the driven Lorenz system by the driving Rossler system. They then misinterpreted this incorrect result to correctly conclude that the Rossler system was causal. (Confusing, but we explain below).

We reanalyze this coupled system using convergent simplex projection (the forecast analogue of CCM) with $\alpha = 6$, as in (*42*)). To obtain robust results that are insensitive to initial starting point, the time series are analyzed using 100 randomly chosen starting points at each L. The ensemble results in Figure S5 for $C = 2.0$, are qualitatively similar for levels of coupling strength (C) below synchrony. Depending on starting point, the relative cross predictability can reverse as one goes from very low values of L (short time series length) to larger L. At low values of L, the error bars overlap and relative cross predictability is sufficiently ambiguous to give reversed cross predictability in the analysis. Interestingly (and confusingly) Le Van Quyen et al. (*42*) based their conclusion about the direction of causation on the (incorrect) direction of relative cross predictability obtained with their forecasting method, and arrived at an "apparently" correct result (multiplied two binary errors to get it right). The correct interpretation is that stronger "convergent" cross prediction by the Lorenz system on the Rossler system indicates that the Rossler system causally forces the Lorenz system, rather than the opposite interpretation given in (*42*). Figure S5, shows that simple cross prediction by itself without considering convergence is not sufficient to identify causation.

<u>Granger causality</u>

As described by Granger (*18*), variable X is said to 'Granger cause' Y if the predictability of the target variable Y declines (signified by higher variance) when X is removed from the universe of all possible causative variables, U. That is to say, X 'Granger causes' Y when

$$\sigma^2\left\{\left(Y|\overline{U}\right)\right\} < \sigma^2\left\{\left(Y|\overline{U-X}\right)\right\} \tag{S8}$$

(The over-bar indicates that only prior values of the causative variables are used for prediction.) The key requirement of Granger is separability, namely that information about causative factors can be subtracted from the effects (as indicated on the right hand side of equation (S8)). Separability is satisfied in linear systems, and GC has been useful for stochastic systems, for linear systems exhibiting stable points or limit cycles, and for detecting interactions between strongly-coupled variables in nonlinear systems.

However, as Granger realized early on (*18*) this approach may be problematic in general nonlinear dynamic systems (especially with weak to moderate coupling). For example, it can be shown that the approach yields ambiguous results for dynamically coupled variables such as those shown in Figure 1 (see below for a detailed analysis). This is because Granger's condition of separability $\left(Y|\overline{U-X}\right)$ is generically unattainable in general dynamic systems (*19, 20*). That is, if X is a cause for Y, complete information about X will be encoded in the target variable Y itself, so that X cannot formally be removed from U – a fact that is essentially a corollary of Takens' Theorem (*19, 20*). Therefore GC is limited to cases where separability can be met; and as Granger himself suspected (*18*), this does not include general dynamic systems. Indeed, when applied to nonseparable systems (where Granger's definition is violated), the GC calculations no longer have a clear relation to causation: leaving vacant the question of detecting causation in such systems (Box S1 contains a simple example illustrating these ideas).

<u>Granger causality methods applied to the time series data used in this work</u>

Here, we summarize results from applying the three main Granger methods (vector autoregression (VAR), spectral decomposition (SD), and conditional mutual information (CMI)) to the three model examples and two empirical examples analyzed in the main text (Table S2). Strictly speaking, because Granger's assumption of separability is not satisfied in this class of examples, such calculations have no necessary connection to causality as defined by Granger. (They belong to a class of system that falls outside of the Granger purview). Thus, a more exhaustive sample of specific methods is not warranted, as the separability issue is independent of any specific method of calculating G-causality (e.g., VAR, spectral, or nonlinear methods). Nonetheless, we include these calculations for heuristic reasons to illustrate the dangers of applying Granger's approach to nonseparable systems for which it was not intended.

The analysis shows that the Granger tests are not robust when the separability assumption is violated. In each case considered here they either consistently misidentify the causal network, give results that are ambiguously sensitive to the choice of test parameters (e.g. lag length, number of Fourier intervals, wavelet base parameter) or give results that vary with time series length. Again, this analysis is not a criticism of the G-causality approach, as these examples fall outside of the Granger purview.

We note that in some of these applications it may be possible to find a choice of test parameters that appear to identify the correct causal network. However, to do so one must know

in advance what the network looks like in order to choose the parameters that produce the correct network (arbitrary fitting). Thus, even if separability did not invalidate these tests (violating the definition of G-causality), the ambiguity of multiple results would make them useful only post-hoc, and not as a way to determine causation a priori when the answer is not already known.

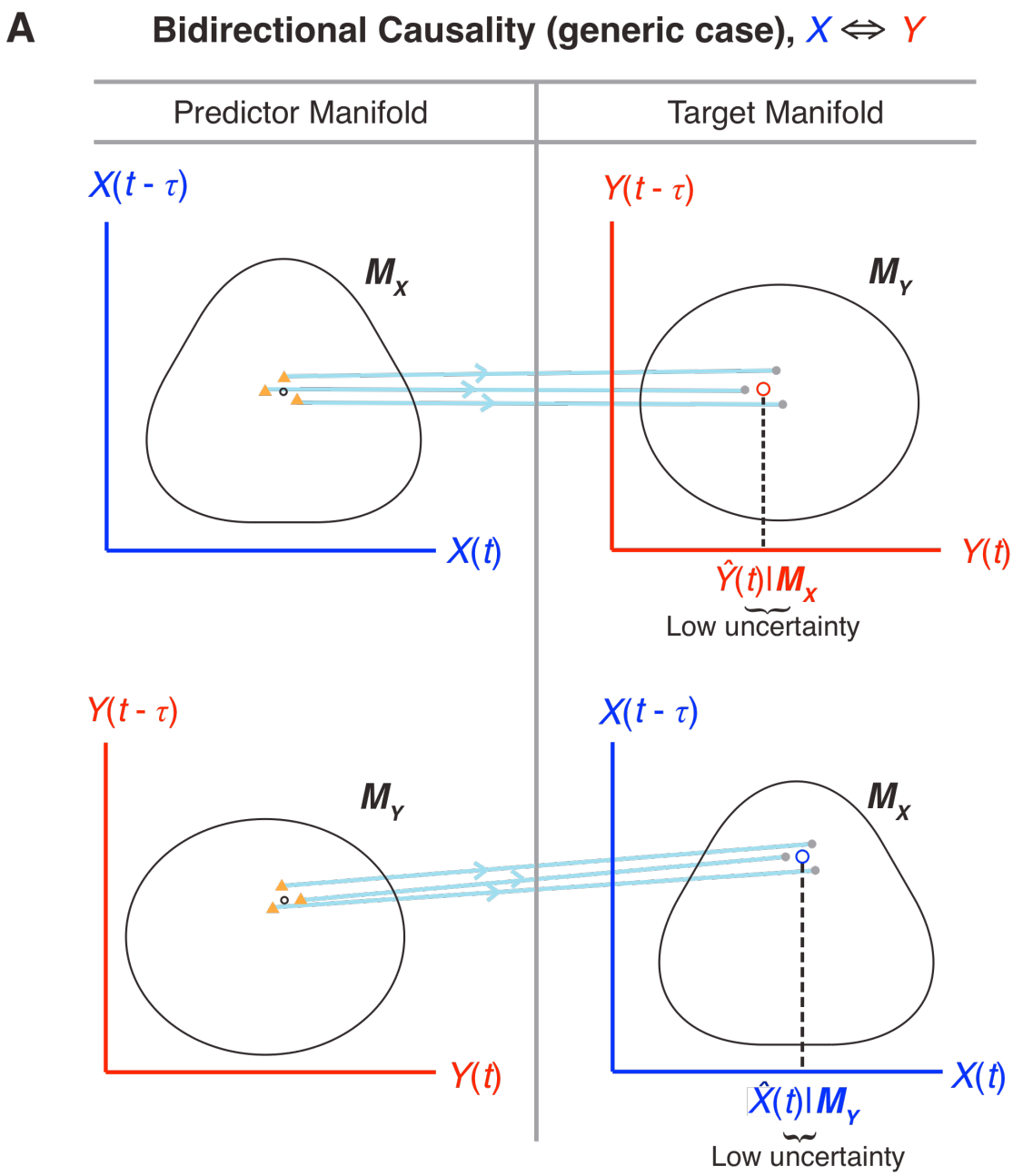

Figure S1A. Cross Mapping

Panel **(A)** shows cross mapping for the generic bidirectional case, where the reconstructed manifold $\boldsymbol{M_X}$ is diffeomorphic to the original manifold and $\boldsymbol{M_Y}$, because the variable X contains information about the dynamics of Y. When making predictions from the predictor $X(t)$ at time t

(represented as a black circle), the nearest points in $\boldsymbol{M_X}$ (orange triangles) are mapped to $\boldsymbol{M_Y}$. On $\boldsymbol{M_Y}$, the centroid of these points is the target prediction (green circle), which gives values for $\hat{Y}(t) \mid \boldsymbol{M_X}$. The range of values for the gray circles corresponds to the uncertainty in prediction. Because these points remain close in the manifold $\boldsymbol{M_Y}$ ($\boldsymbol{M_X}$ is diffeomorphic), the uncertainty is low for predicting $\hat{Y}(t) \mid \boldsymbol{M_X}$, as well as $\hat{X}(t) \mid \boldsymbol{M_Y}$.

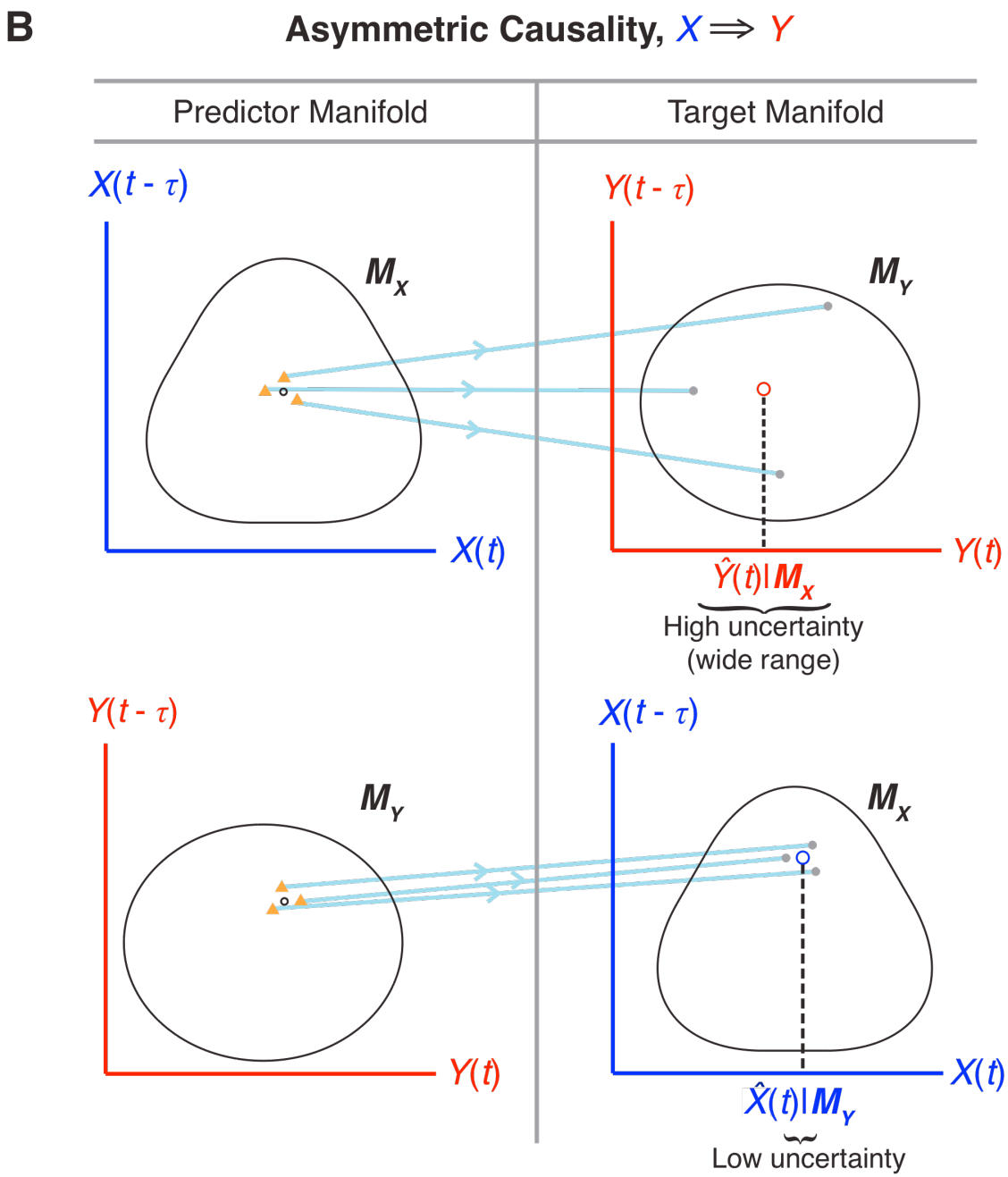

Figure S1B. Cross Mapping

In panel **(B)**, predictions are done as in panel **(A)**, but for the special non-generic case where X is insensitive to the state of Y (i.e. Y does not have any influence on X). Since $\boldsymbol{M_X}$ is not diffeomorphic to $\boldsymbol{M}$ in this situation, the nearest neighbors on $\boldsymbol{M_X}$ (orange triangles) do not map accurately to nearest neighbors on $\boldsymbol{M_Y}$ and are far apart. More specifically, on $\boldsymbol{M_Y}$, the corresponding time-indexed neighbors fail to specify the state (are randomly spread apart on $\boldsymbol{M_Y}$) because X contains incomplete information about the dynamics of Y. Thus, estimating the state $\hat{Y}(t) \mid \boldsymbol{M_X}$ has high uncertainty.

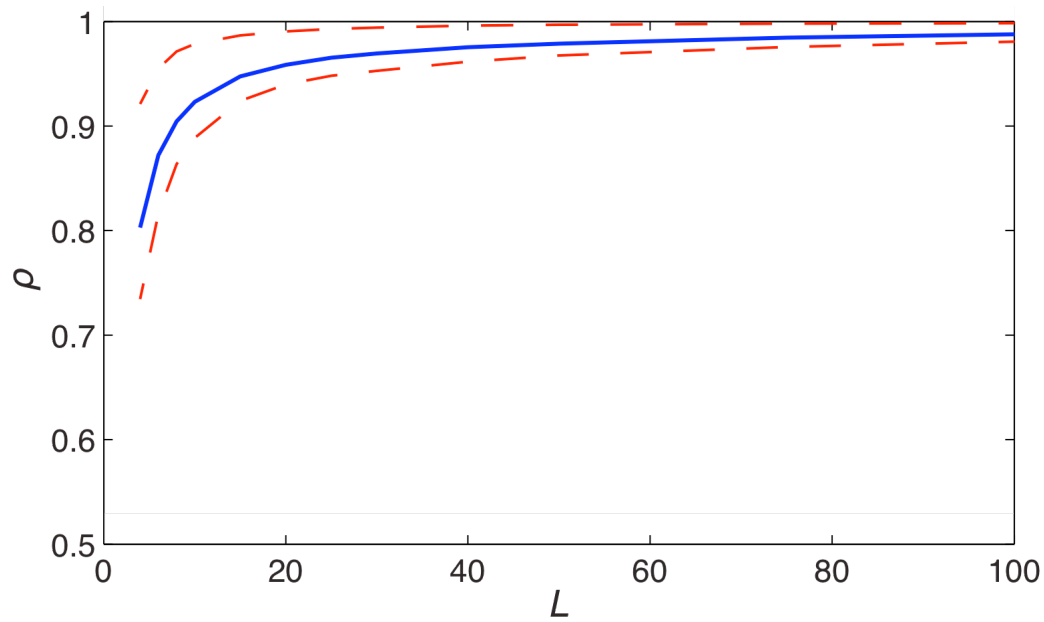

Figure S2. Convergent Predictability with Increasing Time Series Length

Predictive skill increases with time series length (L), and converges to 1 as L approaches infinity. The blue line denotes average ρ (out-of-sample correlation) between 1000 predictions and observations of X and Y (univariate simplex prediction averaged over 3000 trials) using the model in Fig. 1 with randomly chosen coefficients (r and β chosen uniformly in the intervals [3.6, 4.0] and [0, 0.5], respectively). Dashed red lines denote first and third quartiles. As L increases, the density of trajectories in the reconstructed (shadow) manifold ($\boldsymbol{M_X}$ or $\boldsymbol{M_Y}$) increases, and prediction error approaches 0 as ambiguous singularities in the reconstructed manifold decline.

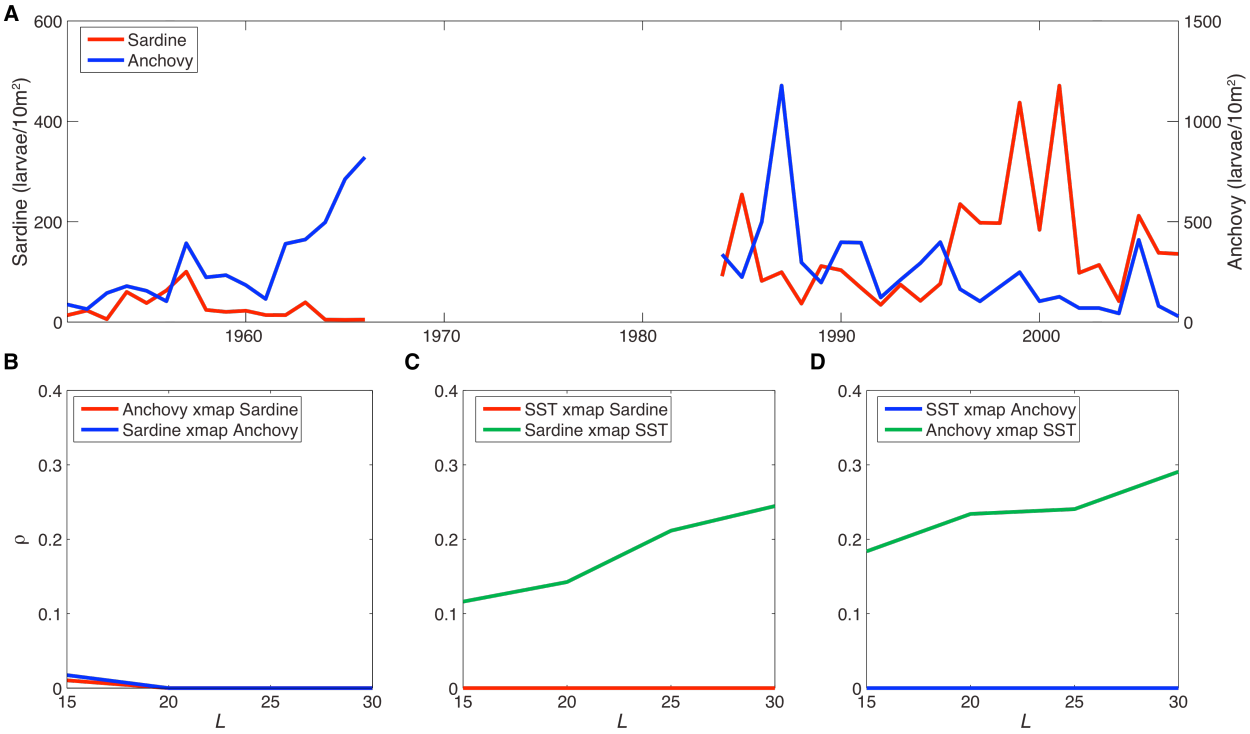

Figure S3. Convergent Cross Mapping using CalCOFI Ichthyoplankton Data

(A) Time series for sardine and anchovy ichthyoplankton in California showing the gap produced during triennial surveys. Panel **(B)** shows a lack of significant CCM between sardines and anchovies. However, asymmetric CCM exists between both populations and SST for the California Current System. **(C)** Sardines show the strongest relationship to Scripps pier SST. **(D)** Anchovies show the strongest relationship to Newport pier SST.

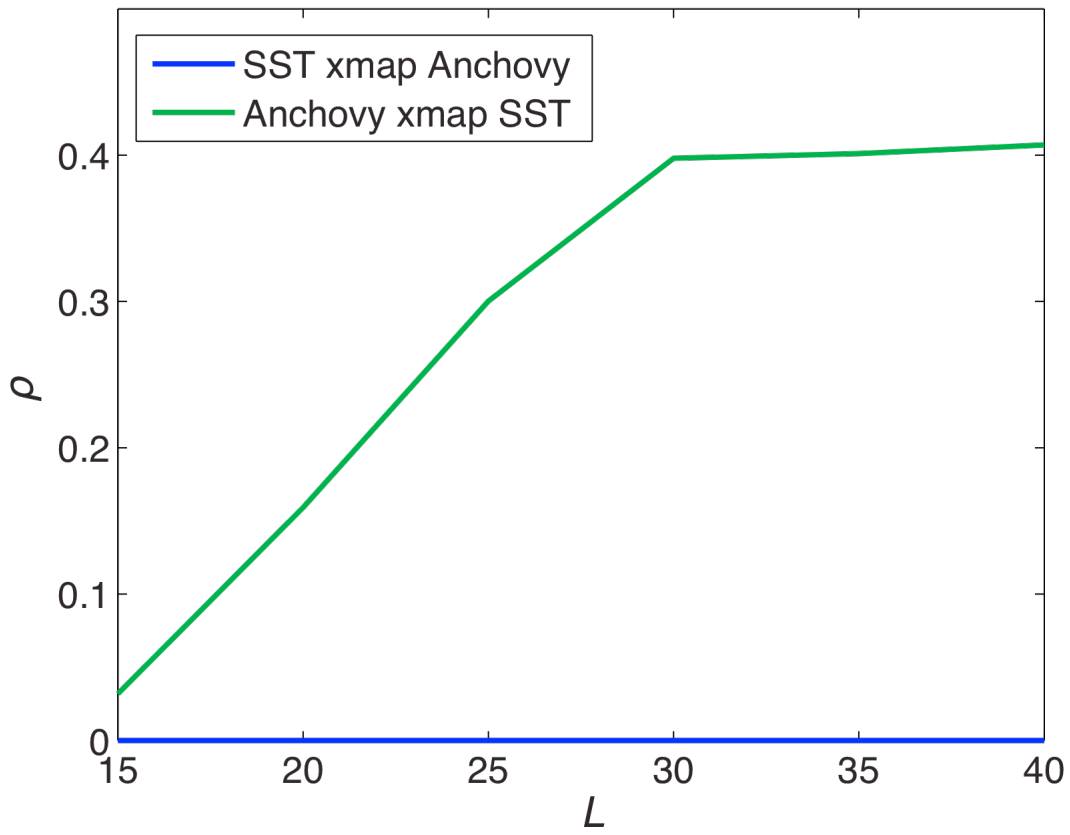

Figure S4. Convergent Cross Mapping using Daily Egg Production Data

Running the CCM analysis using anchovy egg production time series confirms that SST drives the anchovy population size and that anchovy DEP does not affect SST.

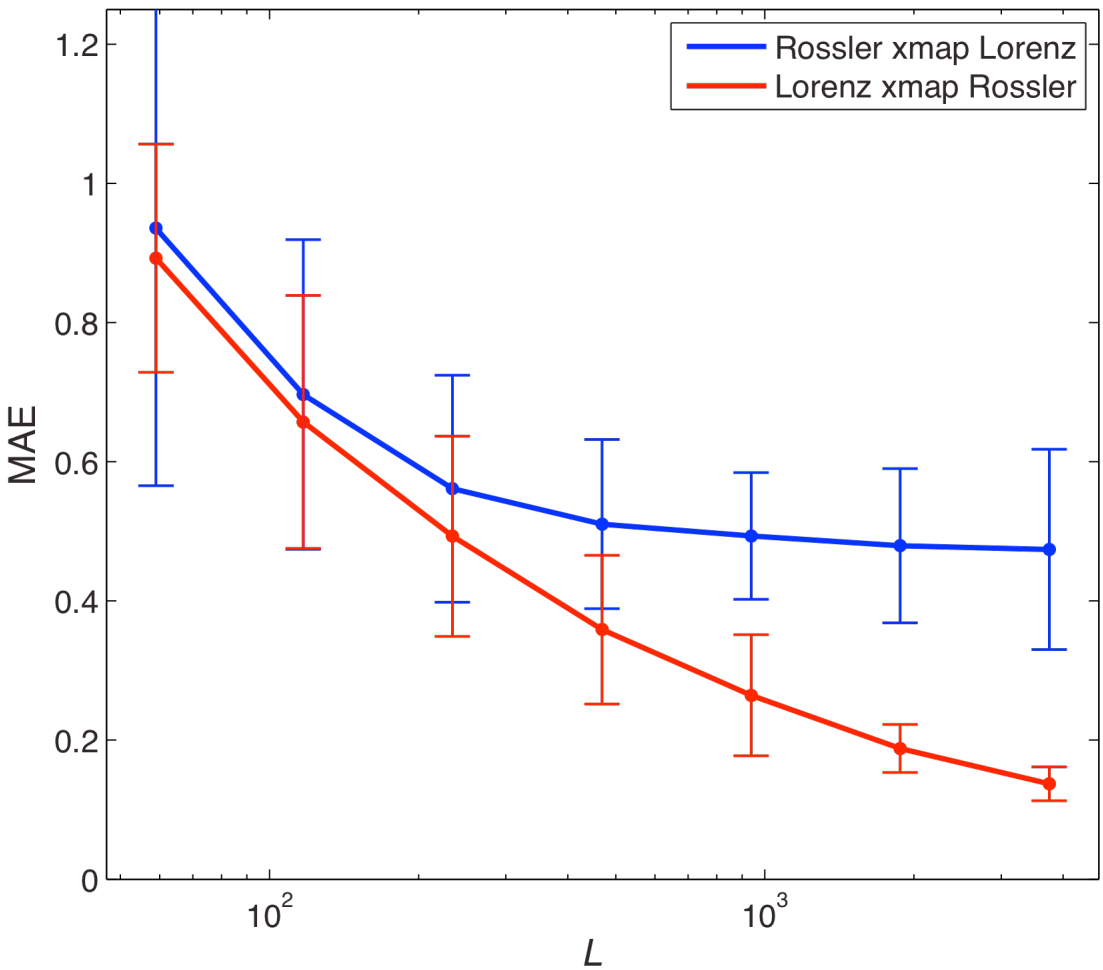

Figure S5. Convergent Cross Mapping for the Rossler-Lorenz Example of (*42*)

Running the CCM analysis for the noise-free Rossler-Lorenz example ($\alpha = 6$, $C = 2$, $E = 13$, tau = 2) of Le Van Quyen et al. (*42*), we also use the MAE error metric. The solid lines are mean values for different possible libraries (starting points). At lower levels of L before convergence, there is ambiguity in the direction of cross predictability for single realizations of the experiment (indicated by the overlap in the 95% error bars). Because this is an error-free model, perfect convergence (zero MAE) will occur with infinite data (see error trend). This analysis, with convergence, correctly shows that the Rossler system causally influences the Lorenz system dynamics but that causation is essentially unidirectional.

Table S1.

Finite convergence results of CCM ($E = 3$, $L = 4000$) for coupled Henon maps ($C = 0.1$, $B = 0.3$) in the model from Schiff et al. (*41*). The nonsignificant (or negative) ρ for $\hat{Y}(t) \mid \boldsymbol{M_X}$ indicates that $\{X\}$ lacks information about the dynamics of Y. Thus, X is not influenced by Y. However, the finite convergence results of CCM (L=4000) clearly demonstrate that $\{Y\}$ contains information about X, Showing that Y is influenced by X. p-values are obtained via comparison with 1000 surrogate time series generated using a power-spectrum preserving technique (*54*).

Cross mapping	$\boldsymbol{\rho}$	***p-value***
$\hat{Y}(t) \mid \boldsymbol{M_X}$	-0.113	NaN
$\hat{X}(t) \mid \boldsymbol{M_Y}$	0.808	< 0.01

Table S2.

Summary table of Granger causality tests applied to the five time series datasets discussed in the main text. L is the time series length. For vector autoregression (VAR) tests, the maximum lag was determined by a likelihood-ratio test. For conditional mutual information (CMI) tests, the modified Baek & Brock (*55*) procedure was used with $\varepsilon = 1.5$, $m = 1$, and $L_X = L_Y = 1$ up to the maximum VAR lag. For the spectral method, we examined 100 Fourier intervals, a wavelet base parameter of 6 (following (*56*)) and 15 (following (*57*)), and a spectral extrapolation limit of 0.02. Significance is tested at the $\alpha < 0.05$ level against 500 iterative amplitude adapted Fourier transform (IAAFT) surrogates (*58*). Results are marked as correct, when the entire causal network is described correctly, and incorrect if the test misidentifies a causal interaction as nonexistent, or a non-interaction as a false positive. Results are marked as inconsistent, when multiple parameter settings are used and only some combinations of parameter settings appear to give the correct causal network.

Dataset	***L***	**Granger causality test**	**Results**
2-species model	300	VAR (max lag = 9)	incorrect
		Spectral (wavelet base number = 6)	incorrect
		Spectral (wavelet base number = 15)	incorrect
		CMI (max lag = 9)	incorrect
	3000	VAR (max lag = 23)	correct
		Spectral (wavelet base number = 6)	correct
		Spectral (wavelet base number = 15)	correct
		CMI (max lag = 23)	inconsistent
Example 1 (2-species externally driven by white noise)	300	VAR (max lag = 5)	correct
		Spectral (wavelet base number = 6)	incorrect
		Spectral (wavelet base number = 15)	correct
		CMI (max lag = 5)	inconsistent
	3000	VAR (max lag = 5)	incorrect
		Spectral (wavelet base number = 6)	incorrect
		Spectral (wavelet base number = 15)	incorrect
		CMI (max lag = 5)	incorrect
Example 2 (5-species model)	300	VAR (max lag = 10)	incorrect
		Spectral (wavelet base number = 6)	incorrect
		Spectral (wavelet base number = 15)	incorrect
		CMI (max lag = 10)	inconsistent
	3000	VAR (max lag = 10*)	incorrect
		Spectral (wavelet base number = 6)	incorrect
		Spectral (wavelet base number = 15)	incorrect
		CMI (max lag = 44)	inconsistent
Didinium-Paramecium (laboratory predator-prey system)	60	VAR (max lag = 1)	incorrect
		Spectral (wavelet base number = 6)	incorrect
		Spectral (wavelet base number = 15)	incorrect
		CMI (max lag = 1)	correct
	74	VAR (max lag = 2)	incorrect

Sardine-anchovy-sea surface temperature (California current ecosystem)✚	74	VAR (max lag = 2)	incorrect
		Spectral (wavelet base number = 6)	no links found
		Spectral (wavelet base number = 15)	no links found
		CMI (max lag = 2)	no links found

*For the VAR test applied to 3000 points of example 2 (5-species model), the likelihood-ratio test suggested a maximum lag of 44, which did not converge. A maximum lag of 10 ran correctly, and those results were used, instead.

✚For the sardine-anchovy dataset, we note that the VAR test suggests that sardines influence sea surface temperature, which is clearly incorrect; for the other tests, no interactions were detected as significant.

GC Calculations S1-S5

Description

Most of the previous work on detecting causality focuses on stochastic and separable systems (including systems that are easily linearized or decomposed in the frequency domain). These methods follow Granger's framework – identifying a variable as causal if it improves predictability (*18*). Applications typically use vector autoregression (VAR) (*59, 60*), conditional mutual information (CMI) (*55, 61-70*), or spectral methods (*16, 57, 71-73*). These methods are well-suited to linear and stochastic systems where tests based on Granger causality apply, but they are not always appropriate for analyzing general dynamic systems (systems where Takens' Theorem applies), and in particular nonlinear systems of diverse components with weak to moderate couplings. Here we describe each of these approaches in detail and apply them to the examples discussed in the main text. We note that because separability is not satisfied in these examples, there is no necessary connection between these test results and causality as defined by Granger. Nonetheless, we believe it is instructive to include them for heuristic reasons. Therefore, rather than a comparative review of skill, this section is intended as a sample involving various methods (including the most frequently used ones) of applying Granger's idea to nonseparable systems.

GC Calculation S1. 2-species model example

<u>Vector autoregression</u>

Vector autoregression with co-integration is the most common test for Granger causality (*59, 60*). We apply this test to time series generated by the dynamic system (1) from the main text consisting of two coupled logistic difference equations (Figure 1) with initial conditions ($X(1) = 0.4$, $Y(1) = 0.2$):

$$X(t+1) = X(t)\,(3.8 - 3.8\,X(t) - 0.02\,Y(t))$$
$$Y(t+1) = Y(t)\,(3.5 - 3.5\,Y(t) - 0.1\,X(t))$$

Although 300 points is an unrealistically long time series in ecology (where time series of 40-60 points (years) are considered long), our aim here is to give a conservatively advantageous demonstration of Granger's method. First, we determine the optimal lag-length through a series of likelihood ratio tests (Table S3), and using the freedom correction factor proposed by Sims (*74*). We choose the largest lag (in this example, 9) for which the likelihood ratio test reports significant degradation in predictability (at the $p < 0.05$ level) for all shorter lags:

Table S3.

Results of likelihood ratio tests for different lag lengths for the time series of X and Y. Because the χ^2 statistic is non-significant for lag 10 vs. lag 9, but significant for all smaller lags, we use a lag length of 9 for analyzing this system.

Test	χ^2 statistic	p-value
lag 12 vs. lag 11	2.608	0.626
lag 11 vs. lag 10	4.458	0.348
lag 10 vs. lag 9	2.457	0.652

lag 9 vs. lag 8	12.655	0.013
lag 8 vs. lag 7	25.851	<0.001
lag 7 vs. lag 6	20.379	<0.001
lag 6 vs. lag 5	35.137	<0.001
lag 5 vs. lag 4	61.885	<0.001
lag 4 vs. lag 3	56.837	<0.001
lag 3 vs. lag 2	109.258	<0.001
lag 2 vs. lag 1	166.963	<0.001

Next, we use Johansen's (*75*) procedure to identify co-integrating relationships (Table S4). Since the time series are naturally bounded between 0 and 1, we only test for a constant term rather than higher-order polynomials in the time series.

Table S4.

Results of the Johansen procedure for identifying co-integrating relationships. The tests determine the significance of r, the number of co-integrating relationships using both the trace statistic (*75*) and the maximal eigenvalue statistic (*76*).

Null	test	test statistic	90% crit. value	95% crit. value	99% crit. value
$r \leq 0$	trace	92.021	13.429	15.494	19.935
$r \leq 1$	trace	30.506	2.705	3.841	6.635
$r \leq 0$	eigenvalue	61.515	12.297	14.264	18.520
$r \leq 1$	eigenvalue	30.506	2.705	3.841	6.635

Since there is significant evidence for co-integration, we use an error-correcting model (*60*) and test for Granger causality using *F*-tests. The models include 9 lags of each variable, as established earlier. Although the tests (Table S5) appear to identify causality from *X* to *Y*, they do not detect the coupling from *Y* to *X*. We believe this is due to the parameterization of the system, which uses a growth rate for species *Y* ($r = 3.5$) that is not in the range for chaotic dynamics ($r > \sim 3.57$). In essence, a linearization around the 4 points of the stable limit cycle does well at capturing the behavior of *Y*, and the lags of *X* can then be used to estimate the perturbations.

We apply this same procedure for using VAR to test for Granger causality in all the later examples, but we report only a summary of the results and include the final table showing p-values.

Table S5.

Results of the Granger causality test using a vector autoregression model for the 2-species model example with 300 points of data. Each cell contains the *p*-value testing that the row column 'Granger causes' the column variable (small values are more significant). Insignificant entries (at the 0.05 level) are indicated by NaN. Results incorrectly indicate unidirectional causality from *X* to *Y* (missing the coupling from *Y* to *X*).

Variable	*X*	*Y*

X	<0.001	<0.001
Y	NaN	<0.001

We repeated the above analysis, but using 3000 points instead. With this amount of data, the VAR analysis found significant evidence for causality in both directions; however, we note that the procedure unreasonably identifies lags of up to 23 as being significant (based on a likelihood-ratio test). Thus, the VAR models contained 49 coefficients (23 coefficients for each variable, two error-correcting terms due to significant co-integration, and a constant term), suggesting that the system is very high-dimensional even though it consists of only two coupled difference-equations with a single lag. This finding is unsurprising, because even though the actual system can be characterized in just a few dimensions, we are attempting to fit a linear model to a nonlinear system with chaotic dynamics. However, this raises concerns about interpreting results when a clearly inappropriate model is being fitted to the data, as well as the data requirements necessary to obtain the correct answer.

Frequency based Granger causality tests

Many authors have also extended the test for Granger causality into the frequency domain (*16, 57*), by decomposing the time series using both Fourier and wavelet transform methods. Here, we test the method described by (*57*), using 100 Fourier intervals, a wavelet base parameter of 6 (following (*56*)) and 15 (following (*57*)), and a spectral extrapolation limit of 0.02. Significance is tested at the $p < 0.05$ level against 500 iterative amplitude adapted Fourier transform (IAAFT) surrogates (*58*).

With 300 points and a wavelet base parameter of 6, the spectral Granger causality test is nonsignificant at all frequencies in the $Y \Rightarrow X$ direction, and significant at 65 out of 100 frequencies in the $X \Rightarrow Y$ direction (Table S6), suggesting asymmetric coupling from *X* to *Y*. Using a wavelet base parameter of 15 generates similar results (Table S6). This result is similar to the VAR results above, and incorrectly detects coupling in only one direction for this system.

Table S6.

Results of the spectral Granger causality test on the 2-species model example with 300 points of data. Table entries give the number of frequencies significant at the 0.05 level against 500 IAAFT surrogates. NA is used here (and in future tables) to indicate a missing value, because the test cannot be used to indicate whether a variable influences itself. Results incorrectly indicate unidirectional causality from *X* to *Y* (missing the coupling from *Y* to *X*) using either 6 or 15 for the wavelet base parameter.

wavelet base parameter = 6		
variable	*X*	*Y*
X	NA	0
Y	65	NA

wavelet base parameter = 15		
variable	*X*	*Y*
X	NA	0
Y	63	NA

Extending the analysis to 3000 points of data, the spectral Granger causality test with a wavelet base parameter of 6 is significant for 46 out of 100 frequencies in the $Y \Rightarrow X$ direction, and 81 out of 100 frequencies in the $X \Rightarrow Y$ direction (Table S7). This test suggests that there is bidirectional causality, though we note that the number of significant frequencies does not necessarily correspond to the relative coupling strength. Using a wavelet base parameter of 15 generates similar results (Table S5). Thus, with an increase in sample size, the apparent causal network changes (which should be disquieting). Again, because of nonseparability, the interpretation that this calculation relates to "causality" *per se* is unclear.

Table S7.

Results of the spectral Granger causality test on the 2-species model example with 3000 points of data. Table entries give the number of frequencies significant at the 0.05 level against 500 IAAFT surrogates.

wavelet base parameter = 6		
variable	*X*	*Y*
X	NA	46
Y	81	NA

wavelet base parameter = 15		
variable	*X*	*Y*
X	NA	28
Y	69	NA

Conditional Mutual Information

There is a large body of work on detecting causality in time series using the concept of conditional mutual information (CMI) and the equivalent concept of transfer entropy (*55, 61-65, 67, 68*). Much of this material has appeared in the last two decades, primarily in the neuroscience and physics literature. Although CMI was apparently developed independently (citations to the earlier work in economics are largely absent in the CMI literature), these statistical methods are mathematically equivalent to the earlier Baek & Brock (*61*) method (economics) in their use of correlation integrals and conditional probability to determine causality under Granger's framework.

Similar to SSR forecasting methods, these methods are based on the idea that past behavior can be used as an indicator for future behavior of the time series (*3*). Consider an E-dimensional vector constructed from successive time lags of Y: $\underline{y}(t, E) = \langle Y(t), Y(t\text{-}1), ..., Y(t\text{-}(E\text{-}1))\rangle$. If we have observed vectors in the past that are similar to the corresponding vector for a specific time, s, the forward trajectory of those vectors may contain useful information about the future values of Y: $\Pr[|Y(t+1) - Y(s+1)| < \varepsilon \mid ||\underline{y}(t, L_Y) - \underline{y}(s, L_Y)|| < \varepsilon] > \Pr[|Y(t+1) - Y(s+1)| < \varepsilon]$ for some $\varepsilon > 0$ and $L_Y \geq 1$. Here, $||\underline{x}||$ is the maximum norm, although any distance metric could potentially be used. Essentially, the fact that past trajectories are close ($||\underline{y}(t, L_Y) - \underline{y}(s, L_Y)|| < \varepsilon$) improves the probability that future values are close ($|Y(t+1) - Y(s+1)| < \varepsilon$).

Extending this idea to Granger Causality, Baek & Brock test (*61*) whether conditioning on the past values of another time series (e.g. X) improves predictability of future values of Y compared to conditioning on Y alone. Thus, if the historical values of X improve forecasts of Y, then X Granger causes Y. For a given L_X and $L_Y \geq 1$, and $\varepsilon > 0$, X Granger causes Y if

$\Pr[|Y(t+1) - Y(s+1)| < \varepsilon \mid \|\underline{x}(t, L_X) - \underline{x}(s, L_X)\| < \varepsilon, \|\underline{y}(t, L_Y) - \underline{y}(s, L_Y)\| < \varepsilon] > \Pr[|Y(t+1) - Y(s+1)| < \varepsilon \mid \|\underline{y}(t, L_Y) - \underline{y}(s, L_Y)\| < \varepsilon]$.

This approach gives ambiguous results for the 2-species system above. Table S8 gives the results for the modified Baek & Brock procedure (*55*) applied systematically to the same 300 points tested above, generated from the system in main text Figure 1.

Table S8.

Results of the test of causality based on Conditional Mutual Information.

Direction	*Lx*	*Ly*	*ε*	*test-statistic*	*p-value*
$X \Rightarrow Y$	1	1	1.5	0.290	0.081
$X \Rightarrow Y$	2	2	1.5	0.432	0.024
$X \Rightarrow Y$	3	3	1.5	0.383	0.018
$X \Rightarrow Y$	4	4	1.5	0.445	0.007
$X \Rightarrow Y$	5	5	1.5	0.516	0.004
$X \Rightarrow Y$	6	6	1.5	0.531	0.003
$X \Rightarrow Y$	7	7	1.5	0.419	0.017
$X \Rightarrow Y$	8	8	1.5	0.484	0.012
$X \Rightarrow Y$	9	9	1.5	0.344	0.040
$Y \Rightarrow X$	1	1	1.5	0.086	0.106
$Y \Rightarrow X$	2	2	1.5	0.063	0.054
$Y \Rightarrow X$	3	3	1.5	0.012	0.107
$Y \Rightarrow X$	4	4	1.5	0.002	0.250
$Y \Rightarrow X$	5	5	1.5	0	NaN
$Y \Rightarrow X$	6	6	1.5	0	NaN
$Y \Rightarrow X$	7	7	1.5	0	NaN
$Y \Rightarrow X$	8	8	1.5	0	NaN
$Y \Rightarrow X$	9	9	1.5	0	NaN

This calculation is sensitive to the choice of parameters L_X, L_Y, and ε, and there is no guide as to how to choose these parameters a priori (except post hoc, choosing the ones that come closest to the known correct answer). In this case, even the post hoc procedure fails: a systematic search over $L_X = L_Y = \{1, 2, \ldots, 9\}$ and $\varepsilon = 1.5$ as suggested by Hiemstra & Jones (*55*) finds no evidence for Granger causality from Y to X at any lag, and causality from X to Y at only some of the tested lags. Indeed one would not expect this test to be successful at identifying causal relationships for the system in main text Figure 1. More importantly, because of nonseparability, any relationships found would have an uncertain relationship to causality as defined by Granger.

Extending the analysis to 3000 points, the test for nonlinear Granger causality remained inconsistent across the different lags tested. For most of the lags ($L_X = L_Y = 3...23$), causality from X to Y was significant, whereas causality from Y to X was significant for only a few lags ($L_X = L_Y = 2...4$). In other words, of the 23 lags tested, only 2 correctly identified causality in both directions. Thus, when conflicting results are obtained, one must know the answer ahead of time to select (post hoc) the lag that gives the correct answer. This illustrates the dangers of applying Granger's approach in nonseparable systems for which it was not intended.

GC Calculation S2. Example 1 (external forcing of two variables by a common driver)

Vector autoregression

As for the 2 species system, we test for Granger causality in example 1 (external forcing of two variables by a common driver – the fisheries model example discussed in the main text) applying VAR. Again, this represents a class of system outside of the separable systems that Granger can suitably address. We use the identical protocol used for the CCM analysis (determine maximum lag, determine number of co-integrating relationships, use error-corrected VAR if appropriate, etc.). The results given below in Table S9 (for N=300) show that VAR can generate results that appear consistent with the true causal interaction network. However, when the data are extended to 3000 points (Table S10), VAR incorrectly finds that Y_2 causes Y_1, which is untrue – increasing the time series length has resulted in a false positive. We note that we can determine the correctness of the VAR results only post hoc because we know the model that generated the data. Nonetheless because of nonsperability, the meaning of these calculations with respect to causation is ultimately uncertain.

Table S9.

Results of the Granger causality test using a vector autoregression model on example 1 with 300 points of data. Each cell represents the p-value testing that the row variable 'Granger causes' the column variable (small values are more significant). Results correctly indicate that variables Y_1 and Y_2 are both influenced by the white noise (*WN*) signal and do not interact with each other. (Note that here as elsewhere entries are for the row variable influencing the column variable, and NaN indicates non-significance).

Variable	Y_1	Y_2	*WN*
Y_1	<0.001	NaN	NaN
Y_2	NaN	<0.001	NaN
WN	<0.001	<0.001	NaN

Table S10.

Results of the Granger causality test using a vector autoregression model on example 1 with 3000 points of data. Each cell represents the p-value testing that the row variable 'Granger causes' the column variable (small values are more significant). Results incorrectly indicate that noninteracting variables Y_1 and Y_2 interact.

Variable	Y_1	Y_2	*WN*
Y_1	<0.001	NaN	NaN
Y_2	0.04	<0.001	NaN
WN	<0.00	<0.001	NaN

(ii) Spectral tests for Granger causality

We repeat the above analysis using the Detto et al. (*57*) implementation of a spectral test for Granger causality (*16*). With 300 points and a wavelet base parameter of 6, the spectral Granger causality test is significant for 23 out of 100 frequencies for Y_1 causing Y_2, as well as for most frequencies for the effect of the white noise forcing on Y_1 and Y_2 (Table S11). These results suggest some influence of Y_1 on Y_2, which is incorrect. When using a wavelet base parameter of

15, the spectral Granger causality test is much better (Table S11) at distinguishing between the influence of the white noise signal on Y_1 and Y_2, and the earlier false positive of Y_1 influencing Y_2.

Table S11.

Results of the spectral Granger causality test on example 1 with 300 points of data. Table entries give the number of frequencies significant at the 0.05 level against 500 IAAFT surrogates. At a wavelet base parameter of 6, results incorrectly suggest unidirectional causality from Y_1 to Y_2, but are otherwise correct. At a wavelet base parameter of 15, results correctly identify the white noise signal as the only source of causal influence in this system.

wavelet base parameter = 6			
variable	Y_1	Y_2	*WN*
Y_1	NA	23	1
Y_2	0	NA	0
WN	64	89	NA

wavelet base parameter = 15			
variable	Y_1	Y_2	*WN*
Y_1	NA	2	0
Y_2	2	NA	0
WN	49	71	NA

Extending the analysis to 3000 points of data, the spectral Granger causality test with a wavelet base parameter of 6 seems to increase the signal strength, while also introducing false positives (Table S12). In particular, the analysis seems to suggest coupling between Y_1 and Y_2 when none exists. Using a wavelet base parameter of 15 generates similar false results (Table S12).

Table S12.

Results of the spectral Granger causality test on example 1 with 3000 points of data. Table entries give the number of frequencies significant at the 0.05 level against 500 IAAFT surrogates. Results incorrectly suggest that Y_1 and Y_2 are interacting at a wavelet base parameter of 6 or 15.

wavelet base parameter = 6			
variable	Y_1	Y_2	*WN*
Y_1	NA	25	5
Y_2	38	NA	6
WN	96	96	NA

wavelet base parameter = 15			
variable	Y_1	Y_2	*WN*
Y_1	NA	18	8
Y_2	18	NA	0
WN	94	95	NA

Here, we did not perform conditional spectral Granger test as suggested in (*57*), because in practice conditional variables cannot be known a priori (one needs to know the answer to do the test). By contrast, CCM requires no such information.

Nonlinear tests for Granger causality

Here we repeat the above analysis using the modified Baek & Brock (*61*) test for nonlinear Granger causality. (Note that Baek & Brock is a CMI test). For each pair of variables, we tested multiple parameter values for L_X and L_Y ($\varepsilon = 1.5$, $L_X = L_Y = 1$ to 5, since 5 was the maximum lag supported by a likelihood-ratio test in the VAR analysis). Table S13 contains the minimum p-value over those 5 different tests for each possible variable pair, using time series of 300 points. While the minimum p-values (considering all parameter combinations) incorrectly suggest that all variables are interacting, some parameter values led to non-significant results. Entries in the table marked with a * indicate that there were both significant and non-significant results for that interaction. The only consistent result is that Y_2 does not influence Y_1. However, there is a not a single lag value that correctly determines that the two biological time series are being influenced by white noise, without also containing false positives suggesting that Y_1 and Y_2 interact, or that the external signal is being influenced by Y_1 or Y_2. Again, the results of this test are ambiguous.

Extending the time series to 3000 points, and repeating the analysis (Table S14) with all the lags tested (up to 5, determined in the same way as above), suggest that Y_1 influences its external driver, and the external driver does not influence Y_1 or Y_2. All the other interactions were inconsistent across lags.

Table S13.

Results of the Baek & Brock test for nonlinear Granger causality (the minimum *p*-values for causality tests taken over the 5 values of the L_X and L_Y parameters) in example 1 (external forcing of two variables by a common driver) with 300 points. Entries with * indicate that *p*-values were both below and above 0.05, depending on parameter settings. This analysis misidentifies the causal network (it suggests that all variables are interacting).

Variable	Y_1	Y_2	*WN*
Y_1	NA	0.023*	0.002*
Y_2	0.282	NA	<0.001*
WN	0.009*	0.022*	NA

Table S14.

Results of the Baek & Brock test for nonlinear Granger causality (the minimum p-values for causality tests taken over the 5 values of the L_X and L_Y parameters) in example 1 (external forcing of two variables by a common driver) with 3000 points. Entries with * indicate that *p*-values were both below and above 0.05, depending on parameter settings. This analysis misidentifies the causal network (it suggests that all variables are interacting).

Variable	Y_1	Y_2	*WN*
Y_1	NA	0.012*	<0.001
Y_2	<0.001*	NA	<0.001*
WN	0.148	0.078	NA

GC Calculation S3. Example 2 (5-species complex model)

Vector autoregression

We test for Granger causality in example 2 (5-species model example) applying VAR to the same length of data (L = 300) used for the CCM analysis. The results given in Table S15 below show that VAR does not correctly identify the causal interaction network. In particular, it suggests that neither Y_2, nor Y_3 have internal dynamics (since they do not influence themselves), and that Y_4 has dynamics that are independent of any other variables.

Table S15.

Results of the test of causality (p-values for Granger causality) based on a vector autoregression model, using 300 points. Results indicate that variables Y_1, Y_2, and Y_3 are coupled, although some links are missing, and that Y_4 is not influenced by any other variable. The tests also incorrectly indicate that the only other variable influence on Y_5 is Y_2.

Variable	Y_1	Y_2	Y_3	Y_4	Y_5
Y_1	<0.001	<0.001	<0.001	NaN	NaN
Y_2	<0.001	NaN	NaN	NaN	<0.001
Y_3	<0.001	<0.001	NaN	NaN	NaN
Y_4	NaN	NaN	NaN	<0.001	NaN
Y_5	NaN	NaN	NaN	NaN	<0.001

We attempted to extend this analysis to time series of 3000 points, just as we did with the previous examples. However, the likelihood-ratio test suggested that we needed to include up to 44 lags of each variable, which resulted in errors when fitting the VAR model. Using fewer lags (maximum lag = 10) allowed the model to converge, with results in Table S16. However, we note that 10 lags suggest that the system is very high dimensional, and is thus inappropriate for detecting causality in this case. The results match the true system better than using just 300 points (since Y_1, Y_2, and Y_3 are fully coupled), but the test now detects causality between Y_4 and Y_5, which is incorrect.

Table S16.

Results of the test of causality (p-values for Granger causality) based on a vector autoregression model, using 3000 points. Results indicate that variables Y_1, Y_2, and Y_3 are fully coupled, that Y_2 is the only external influence on Y_5, and that Y_5 is the only external influence on Y_4.

Variable	Y_1	Y_2	Y_3	Y_4	Y_5
Y_1	<0.001	<0.001	<0.001	NaN	NaN
Y_2	<0.001	0.02	0.04	NaN	0.00
Y_3	<0.001	<0.001	<0.001	NaN	NaN
Y_4	NaN	NaN	NaN	<0.001	NaN
Y_5	NaN	NaN	NaN	0.05	<0.001

Spectral tests for Granger causality

We repeat the above analysis using the Detto et al. (*57*) implementation of a spectral test for Granger causality. With 300 points and a wavelet base parameter of 6, the spectral Granger

causality test finds most of the variable interactions between Y_1, Y_2, and Y_3 to be significant at a reasonable proportion of frequencies (Table S17). However, the test also suggests a strong causal influence of Y_4 on Y_1 and Y_3, which is incorrect, and indicates that no variables influence Y_4 and Y_5. When using a wavelet base parameter of 15, results are similar (Table S17).

Table S17.

Results of the spectral Granger causality test on example 2 with 300 points of data. Table entries give the number of frequencies significant at the 0.05 level against 500 IAAFT surrogates. Results are similar using a wavelet base parameter of 6 or 15, and incorrectly suggest a lack of forcings on Y_4 and Y_5 from Y_1, Y_2, or Y_3, as well as indicating that Y_4 influences Y_1 and Y_3.

wavelet base parameter = 6					
variable	Y_1	Y_2	Y_3	Y_4	Y_5
Y_1	NA	52	25	8	5
Y_2	30	NA	30	0	0
Y_3	8	30	NA	3	4
Y_4	44	0	41	NA	0
Y_5	0	0	0	5	NA

wavelet base parameter = 15					
variable	Y_1	Y_2	Y_3	Y_4	Y_5
Y_1	NA	42	35	0	2
Y_2	26	NA	41	1	2
Y_3	26	36	NA	5	2
Y_4	36	3	15	NA	2
Y_5	6	3	4	11	NA

Extending the analysis to 3000 points of data, the spectral Granger causality test with a wavelet base parameter of 6 (Table S18) suggests that there are only a few interactions, mostly between Y_1, Y_2, and Y_3. Although the test does indicate that there may be a weak effect of Y_1 on Y_4, this is about the same level as the effect of Y_5 on Y_4 (incorrect) and Y_5 on Y_1 (also incorrect). Using a wavelet base parameter of 15 generates similar results (Table S18). The spectral test does better at suggesting that Y_2 causes Y_5, but still misses a majority of the influence of Y_1, Y_2, and Y_3 on Y_4 and Y_5, in addition to (incorrectly) suggesting that there might be a weak effect of Y_4 on Y_2 and Y_5 on Y_4.

Table S18.

Results of the spectral Granger causality test on example 2 with 3000 points of data. Table entries give the number of frequencies significant at the 0.05 level against 500 IAAFT surrogates. Using a wavelet base parameter of 6, only a few interactions appear to be significant, and it is difficult to distinguish between the true effects of Y_2 on Y_3 and the false positive of the effect of Y_5 on Y_4. Using a wavelet base parameter of 15, the forcings between Y_1, Y_2, and Y_3 appear more strongly, but so do the false positive signals (Y_4 influences Y_2 or Y_5 influencing Y_4).

wavelet base parameter = 6					
variable	Y_1	Y_2	Y_3	Y_4	Y_5

Y_1	NA	1	17	12	3
Y_2	28	NA	10	1	2
Y_3	1	21	NA	1	3
Y_4	0	2	0	NA	0
Y_5	9	0	0	11	NA

wavelet base parameter = 15					
variable	Y_1	Y_2	Y_3	Y_4	Y_5
Y_1	NA	15	30	3	7
Y_2	64	NA	36	6	29
Y_3	46	24	NA	10	4
Y_4	6	16	5	NA	2
Y_5	4	1	4	15	NA

Nonlinear Tests for Granger causality

Here we repeat the above analysis using the modified Baek & Brock (*61*) test for nonlinear Granger causality. For each pair of variables, we tested multiple parameter values for L_X and L_Y ($\varepsilon = 1.5$, $L_X = L_Y = 1$ to 10, since 10 was the maximum lag supported by a likelihood-ratio test in the VAR analysis). Table S19 contains the minimum p-value over those 10 different tests for each possible variable pair. While the minimum p-value suggests many interactions, some parameter values led to non-significant results. Entries in the table marked with a * indicate that there were both significant and non-significant results for that variable interaction. Over the 10 different lag lengths, each pairwise interaction is significant at some point. Furthermore, only some of the interactions between Y_1, Y_2, and Y_3 were significant at each parameter setting. Thus the test is partially successful at resolving the network of interactions among Y_1, Y_2, and Y_3, but cannot adequately distinguish between false positives and true interactions for the weaker couplings (the effects of Y_1, Y_2, and Y_3 on Y_4 and Y_5) in the system.

We extend the analysis by testing for nonlinear Granger causality on 3000 point time series from the same system (Table S19). Using lags up to 44 (as determined by the likelihood-ratio test from the VAR analysis on the same data), all interactions are significant at some parameter settings. The only interactions that were significant at all parameter settings were 3 of the 6 interactions between Y_1, Y_2, and Y_3. Thus, of the 12 true interactions in the system, 3 were identified consistently, and of the 8 non-interactions in the system, all 8 were falsely identified as significant interactions for some lag.

Table S19.

Results of the Baek & Brock test for nonlinear Granger causality (the minimum *p*-values for causality tests taken over the 10 values of the L_X and L_Y parameters) in the 5-species model system, with 300 points. As with the results from the vector autoregression analysis above, this analysis misidentifies the causal network (the only consistently identified causal links are between Y_1, Y_2, and Y_3, but only 4 of the possible 6 are consistently significant)).

Variable	Y_1	Y_2	Y_3	Y_4	Y_5
Y_1	NA	<0.001	<0.001*	0.023*	0.008*
Y_2	<0.001*	NA	<0.001	0.046*	0.025*
Y_3	<0.001	0.000	NA	0.026	0.042*

Y_4	0.038*	0.041*	0.040*	NA	<0.001*
Y_5	<0.001*	<0.001*	<0.001*	<0.001*	NA

Table S20.

Results of the Baek & Brock test for nonlinear Granger causality (the minimum p-values for causality tests taken over the 44 values of the L_X and L_Y parameters) in the 5-species model system, with 3000 points. All interactions are significant at some lag value, but only 3 of 12 actual connections are identified consistently.

Variable	Y_1	Y_2	Y_3	Y_4	Y_5
Y_1	NA	<0.001	<0.001*	<0.001*	<0.001*
Y_2	<0.001*	NA	<0.001*	<0.001*	<0.001*
Y_3	<0.001	<0.001	NA	<0.001*	<0.001*
Y_4	<0.001*	<0.001*	<0.001*	NA	<0.001*
Y_5	<0.001*	<0.001*	<0.001*	<0.001*	NA

GC Calculation S4. *Didinium-Paramecium* system

Vector autoregression

We test for Granger causality in the *Didinium-Paramecium* system applying VAR to the same experimental dataset (*17*) used for the CCM analysis. The results in Table S21 show that VAR does not correctly identify the causal interaction network. In fact, it fails to find any interactions at all!

Table S21.

Results of the test of causality (*p*-values for Granger causality) based on a vector autoregression model. Results indicate falsely that there is no interaction between *Paramecium* and *Didinium*.

Variable	*Paramecium*	*Didinium*
Paramecium	NaN	NaN
Didinium	NaN	NaN

Spectral tests for Granger causality

We repeat the above analysis using the Detto et al. (*57*) implementation of a spectral test for Granger causality. With 300 points and a wavelet base parameter of 6, the test identifies an effect of *Paramecium* on *Didinium* (Table S22), but finds significance for only 6 out of 100 frequencies when testing the effect of *Didinium* on *Paramecium*, which is roughly in the range of the non-interactions discussed above. Using a wavelet base parameter of 15, the test suggests no interaction at all between *Paramecium* and *Didinium* (Table S22).

Table S22.

Results of the spectral Granger causality test on the *Didinium-Paramecium* predator-prey system. Table entries give the number of frequencies significant at the 0.05 level against 500 IAAFT surrogates. Using a wavelet base parameter of 6, results suggests that the system is controlled entirely by bottom-up forcing, by only detecting unidirectional causality from *Paramecium* to

Didinium. Using a wavelet base parameter of 15, results indicate that there is no interaction between *Paramecium* and *Didinium*.

wavelet base parameter = 6		
variable	*Paramecium*	*Didinium*
Paramecium	NA	22
Didinium	6	NA

wavelet base parameter = 15		
variable	*Paramecium*	*Didinium*
Paramecium	NA	6
Didinium	1	NA

Nonlinear Tests for Granger causality

Here we repeat the above analysis using the modified Baek & Brock (*55*) test for nonlinear Granger causality. For each pair of variables, we tested values for L_X and L_Y up to the maximum lag indicated by the likelihood-ratio test in the VAR analysis (in this case, the use of only 1 lag). The other parameters were the same as the above analyses ($\varepsilon = 1.5$). Table S23 contains the p-value for the interactions. We note that the test is successful in this instance, and identifies bidirectional coupling between *Paramecium* and *Didinium*. However, unlike the CCM analysis, this measure of significance cannot quantify the asymmetry of coupling.

Table S23.

Results of the modified Baek & Brock test for nonlinear Granger causality (the *p*-values for causality tests for the influence of the row variable on the column variable). The test is successful at identifying causality between the two variables, but provides no measure of possible asymmetry in the coupling strengths.

Variable	*Paramecium*	*Didinium*
Paramecium	NaN	0.006
Didinium	0.004	NaN

GC Calculation S5. Sardine-anchovy system

Vector autoregression

We test for Granger causality in the sardine-anchovy system applying VAR to the same dataset (landings data for Pacific sardine and Northern anchovy, and sea-surface temperature measured at Scripps Pier and Newport Pier) used for the CCM analysis. The results given in Table S24 below show that VAR does not correctly identify the causal interaction network. In particular, it fails to identify any dynamics in the biological variables, but incorrectly finds that sardines influence both sea surface temperature variables.

Table S24.

Results of the test of causality (*p*-values for Granger causality) based on a vector autoregression model. Results strangely indicate that sardine is a driver of sea surface temperatures and that there are no other dynamics in the system.

Variable	*Anchovy*	*Sardine*	*NP SST*	*SIO SST*
Anchovy	NaN	NaN	NaN	NaN
Sardine	NaN	NaN	0.02	0.04
NP SST	NaN	NaN	NaN	NaN
SIO SST	NaN	NaN	NaN	NaN

Spectral tests for Granger causality

We repeat the above analysis using the Detto et al. (*57*) implementation of a spectral test for Granger causality. With a wavelet base parameter of 6, the test identifies no causal interaction in the sardine-anchovy-sea surface temperature system (Table S25). Using a wavelet base parameter of 15, the results are similar (Table S25), though test suggests some evidence for the effect of sea surface temperature on sardines.

Table S25.

Results of the spectral Granger causality test on the sardine-anchovy-sea surface temperature system. Table entries give the number of frequencies significant at the 0.05 level against 500 IAAFT surrogates. Using a wavelet base parameter of 6, results suggest that there are no causal interactions between variables in this system. Using a wavelet base parameter of 15, results suggest that there might be some effect of sea surface temperature on sardines, but no other causal interactions between variables in this system

wavelet base parameter = 6				
variable	*Anchovy*	*Sardine*	*NP SST*	*SIO SST*
Anchovy	NA	1	2	1
Sardine	1	NA	1	0
NP SST	1	1	NA	1
SIO SST	1	1	2	NA

wavelet base parameter =15				
variable	*Anchovy*	*Sardine*	*NP SST*	*SIO SST*
Anchovy	NA	4	2	1
Sardine	3	NA	1	1
NP SST	2	10	NA	7
SIO SST	1	8	4	NA

Nonlinear Tests for Granger causality

Here we repeat the above analysis using the modified Baek & Brock (*55*) test for nonlinear Granger causality. For each pair of variables, we tested multiple parameter values for L_X and L_Y ($L_X = L_Y = 1$ to 2 $\varepsilon = 1.5$). Table S26 contains the minimum p-value over those 2 different tests for each possible variable pair. No interactions were found to be significant at any of the lag lengths tested, though the influence of Newport Pier SST on SIO Pier SST is marginally significant ($p < 0.1$).

Table S26.

Results of the Baek & Brock test for nonlinear Granger causality (the minimum *p*-values for causality taken over the 2 values of the L_X and L_Y parameters). No interactions were found to be significant.

Variable	*Anchovy*	*Sardine*	*NP SST*	*SIO SST*
Anchovy	NA	0.956	0.903	0.857
Sardine	0.985	NA	0.664	0.721
NP SST	0.306	0.124	NA	0.088
SIO SST	0.357	0.259	0.139	NA

Movie S1

This movie demonstrates the relationship between time series and dynamic attractors (manifolds, $\boldsymbol{M}$).

Movie S2

This movie illustrates how Takens' Theorem (*19*) can be used to reconstruct a shadow manifold $\boldsymbol{M_X}$ from a single time series, and illustrates the 1:1 mapping between $\boldsymbol{M}$ and $\boldsymbol{M_X}$.

Movie S3

This movie explains how convergent cross mapping (CCM) estimates states across variables.

Higher resolution versions of these Movies are available at:
http://simplex.ucsd.edu/Movie_S1.mov
http://simplex.ucsd.edu/Movie_S2.mov
http://simplex.ucsd.edu/Movie_S3.mov

Box S1. Building intuition for nonseparability with a simple example

One of the fundamental ideas in this work is that when causation is unilateral, $X \Rightarrow Y$ (X drives Y as in case *ii*), then it is possible to estimate X from Y, but not Y from X. This runs counter to intuition (and Granger causality), and suggests that if the weather drives fish populations, we can use fish to predict the weather but not vice versa. Note that CCM does not involve forecasting *per se*, but predicts (estimates) contemporaneous or past states of causative variables. Thus, if the fish time series contains historical information (in its lags) that allows one to estimate past weather states, this information (the weather information relevant to fish) would be entirely redundant if weather was explicitly added to a model for predicting fish. Thus weather would (incorrectly) not be seen as causative in Granger's scheme, since it could be added or removed from the model with no effect. Nonseparability arises from the redundant causative information already fully contained in the affected variables (a consequence of Takens' theorem).

To further clarify how this works, consider the following special case of the 2-species logistic model:

$$\begin{aligned} X(t+1) &= 3.9\, X(t)\, [1 - X(t) - \beta\, Y(t)] \\ Y(t+1) &= 3.7\, Y(t)\, [1 - Y(t) - 0.2\, X(t)] \end{aligned} \tag{B1}$$

The parameter β governs the sensitivity of X to changes in Y. When β is large, Y strongly reduces growth in X and when $\beta = 0$, X is independent of Y (the dynamics of X do not depend on Y). In this simple system, where we can determine lagged-coordinate models algebraically, we can use the value of $Y(t+1)$ and $Y(t)$ to recover the influence, and thus the value, of $X(t)$ (and vice-versa):

$$\begin{aligned} \beta\, Y(t) &= 1 - X(t) - X(t+1)\, /3.9\, X(t) \\ 0.2\, X(t) &= 1 - Y(t) - Y(t+1)\, /\, 3.7\, Y(t) \end{aligned} \tag{B2}$$

To recover the cross map dynamics (note that equation (B2) alone is insufficient, since it requires future knowledge!), we can simply substitute equation (B2) into (B1) and obtain equations for $X(t)$ in terms of $Y(t)$ and $Y(t\text{-}1)$ and vice-versa:

$$\begin{aligned} X(t) &= \frac{3.9}{0.2}\left\{(1-\beta Y(t-1))\left(1 - Y(t-1) - \frac{Y(t)}{3.7Y(t-1)}\right) - \frac{1}{0.2}\left(1 - Y(t-1) - \frac{Y(t)}{3.7Y(t-1)}\right)^2\right\} \\ Y(t) &= \frac{3.7}{\beta}\left\{(1-0.2X(t-1))\left(1 - X(t-1) - \frac{X(t)}{3.9X(t-1)}\right) - \frac{1}{\beta}\left(1 - X(t-1) - \frac{X(t)}{3.9X(t-1)}\right)^2\right\} \end{aligned} \tag{B3}$$

Note that as β approaches 0, the cross map estimate of X remains well-behaved. But for Y there is a singularity, as the cross map model for Y blows up when $\beta = 0$. This follows directly from equation (B2), where it is clear that there is no way to solve for Y in terms of X when $\beta = 0$. Informally, when $\beta = 0$, X moves through the state-space without regard to the current location of Y. Therefore the history of X is irrelevant for determining Y.

Additionally, in the bidirectional case ($\beta \neq 0$), (B3) can be substituted back into (B1) to obtain an equation for $X(t+1)$ purely in terms of $X(t)$ and $X(t-1)$. Thus, even though X and Y are coupled, we can write an exact model for predicting X on the basis of its past history alone (i.e. without including any observations of Y). However, in the GC framework, because Y can be removed from the set of hypothetical causal variables without diminishing the predictability of X, we would conclude (incorrectly!) that Y does not cause X.

This simple model also provides another argument for why convergence of cross-mapped estimates is a necessary condition for detecting causality and for why the rate of convergence provides an index of interaction strength. To see this, note that to first order, (B3) indicates that the variance in Y is proportional to $\mathrm{Var}(X)/\beta^2$. Because cross map estimates for Y are based on the nearest neighbors of X, the uncertainty in Y will be large whenever the neighborhood for X is large. As the attractor fills in with increasing time series length, the nearest-neighborhoods become smaller, and the variance in Y decreases. Thus, the variance in Y is a function of the interaction strength; to obtain the same precision requires more data when β is small than when β is large.

References

1. G. Berkeley, *A Treatise on Principles of Human Knowledge* (1710).

2. M. Casini *et al*., Trophic cascades promote threshold-like shifts in pelagic marine ecosystems. *Proc. Natl. Acad. Sci. U.S.A.* **106**, 197 (2009). doi:10.1073/pnas.0806649105 Medline

3. G. Sugihara, R. M. May, Nonlinear forecasting as a way of distinguishing chaos from measurement error in time series. *Nature* **344**, 734 (1990). doi:10.1038/344734a0 Medline

4. P. A. Dixon, M. J. Milicich, G. Sugihara, Episodic fluctuations in larval supply. *Science* **283**, 1528 (1999). doi:10.1126/science.283.5407.1528 Medline

5. W. A. Brock, C. L. Sayers, Is the business cycle characterized by deterministic chaos? *J. Monet. Econ.* **22**, 71 (1988). doi:10.1016/0304-3932(88)90170-5

6. B. T. Grenfell *et al*., Noise and determinism in synchronized sheep dynamics. *Nature* **394**, 674 (1998). doi:10.1038/29291

7. A. Mysterud, N. C. Stenseth, N. G. Yoccoz, R. Langvatn, G. Steinheim, Nonlinear effects of large-scale climatic variability on wild and domestic herbivores. *Nature* **410**, 1096 (2001). doi:10.1038/35074099 Medline

8. C. H. Hsieh, S. M. Glaser, A. J. Lucas, G. Sugihara, Distinguishing random environmental fluctuations from ecological catastrophes for the North Pacific Ocean. *Nature* **435**, 336 (2005). doi:10.1038/nature03553 Medline

9. G. I. Bischi, C. Chiarella, L. Gardini, Eds., *Nonlinear Dynamics in Economics, Finance and Social Sciences* (Springer, Berlin, 2010).

10. D. A. S. Patil, B. R. Hunt, J. A. Carton, Identifying low-dimensional nonlinear behavior in atmospheric data. *Mon. Weather Rev.* **129**, 2116 (2001). doi:10.1175/1520-0493(2001)129<2116:ILDNBI>2.0.CO;2

11. T. T. Lo, H. H. Hsu, Change in the dominant decadal patterns and the late 1980s abrupt warming in the extratropical Northern Hemisphere. *Atmos. Sci. Lett.* **11**, 210 (2010). doi:10.1002/asl.275

12. X. Rodo, M. Pascual, G. Fuchs, A. S. G. Faruque, ENSO and cholera: A nonstationary link related to climate change? *Proc. Natl. Acad. Sci. U.S.A.* **99**, 12901 (2002). doi:10.1073/pnas.182203999 Medline

13. B. K. Wagner *et al*., Large-scale chemical dissection of mitochondrial function. *Nat. Biotechnol.* **26**, 343 (2008). doi:10.1038/nbt1387 Medline

14. A. L. Lloyd, The coupled logistic map: A simple model for the effects of spatial heterogeneity on population dynamics. *J. Theor. Biol.* **173**, 217 (1995). doi:10.1006/jtbi.1995.0058

15. Committee on Major U.S. Oceanographic Research Programs, National Research Council, *Global Ocean Science: Toward an Integrated Approach* (National Academies Press, Washington, DC, 1999).

16. Y. Chen, S. L. Bressler, M. Ding, Frequency decomposition of conditional Granger causality and application to multivariate neural field potential data. *J. Neurosci. Methods* **150**, 228 (2006). doi:10.1016/j.jneumeth.2005.06.011 Medline

17. R. M. May, S. A. Levin, G. Sugihara, Complex systems: Ecology for bankers. *Nature* **451**, 893 (2008). doi:10.1038/451893a Medline

18. C. W. J. Granger, Investigating causal relations by econometric models and cross-spectral methods. *Econometrica* **37**, 424 (1969). doi:10.2307/1912791

19. F. Takens, in *Dynamical Systems and Turbulence*, D. A. Rand, L. S. Young, Eds. (Springer-Verlag, New York, 1981), pp. 366–381.

20. E. R. Deyle, G. Sugihara, Generalized theorems for nonlinear state space reconstruction. *PLoS ONE* **6**, e18295 (2011). doi:10.1371/journal.pone.0018295 Medline

21. K. McCann, A. Hastings, G. R. Huxel, *Nature* **395**, 794 (1998). doi:10.1038/27427

22. C. H. Hsieh *et al*., Time series analyses reveal transient relationships between abundance of larval anchovy and environmental variables in the coastal waters southwest of Taiwan. *Fish. Oceanogr.* **18**, 102 (2009). doi:10.1111/j.1365-2419.2008.00498.x

23. P. A. P. Moran, The statistical analysis of the Canadian Lynx cycle. *Aust. J. Zool.* **1**, 291 (1953). doi:10.1071/ZO9530291

24. N. H. Packard, J. P. Crutchfield, J. D. Farmer, R. S. Shaw, Geometry from a time series. *Phys. Rev. Lett.* **45**, 712 (1980). doi:10.1103/PhysRevLett.45.712

25. F. A. Ascioti, E. Beltrami, T. O. Carroll, C. Wirick, Is there chaos in plankton dynamics? *J. Plankton Res.* **15**, 603 (1993). doi:10.1093/plankt/15.6.603

26. See supplementary materials on *Science* Online.

27. K. Josic, Synchronization of chaotic systems and invariant manifolds. *Nonlinearity* **13**, 1321 (2000). doi:10.1088/0951-7715/13/4/318

28. B. G. Veilleux, thesis, University of Alberta (1976).

29. R. A. Schwartzlose *et al*., Worldwide large-scale fluctuations of sardine and anchovy populations. *S. Afr. J. Mar. Sci.* **21**, 289 (1999). doi:10.2989/025776199784125962

30. G. I. Murphy, J. D. Isaacs, Species replacement in marine ecosystems with reference to the California current. *Minutes of Meeting Marine Research Committee* **7**, 1 (1964).

31. R. Lasker, A. MacCall, New ideas on the fluctuations of the clupeoid stocks off California. In *Proceedings of the Joint Oceanographic Assembly, Halifax, August 1982: General Symposia* (Department of Fisheries and Oceans, Ontario, 1983), pp. 110–120.

32. T. R. Baumgartner, A. Soutar, V. Ferreira-Bartrina, *CCOFI Rep.* **33**, 24 (1992).

33. L. D. Jacobson, A. D. MacCall, Stock-recruitment models for Pacific sardine (*Sardinops sagax*). *Can. J. Fish. Aquat. Sci.* **52**, 566 (1995). doi:10.1139/f95-057

34. S. McClatchie, R. Goericke, G. Auad, K. Hill, Re-assessment of the stock-recruit and temperature-recruit relationships for Pacific sardine (*Sardinops sagax*). *Can. J. Fish. Aquat. Sci.* **67**, 1782 (2010). doi:10.1139/F10-101

35. J. P. Crutchfield, thesis, University of California, Santa Cruz (1979).

36. T. Sauer, J. A. Yorke, M. Casdagli, Embedology. *J. Stat. Phys.* **65**, 579 (1991). doi:10.1007/BF01053745

37. W. M. Schaffer, Stretching and folding in lynx fur returns: Evidence for a strange attractor in nature? *Am. Nat.* **124**, 798 (1984). doi:10.1086/284318

38. M. Casdagli, Nonlinear prediction of chaotic time series. *Physica D* **35**, 335 (1989). doi:10.1016/0167-2789(89)90074-2

39. D. Ruelle, *Chaotic Evolution and Strange Attractors: The Statistical Analysis of Time Series for Deterministic Nonlinear Systems* (Cambridge Univ. Press, Cambridge, 1989).

40. C. H. Hsieh, C. Anderson, G. Sugihara, Extending nonlinear analysis to short ecological time series. *Am. Nat.* **171**, 71 (2008). doi:10.1086/524202 Medline

41. S. J. Schiff, P. So, T. Chang, R. E. Burke, T. Sauer, Detecting dynamical interdependence and generalized synchrony through mutual prediction in a neural ensemble. *Phys. Rev. E* **54**, 6708 (1996). doi:10.1103/PhysRevE.54.6708 Medline

42. M. Le Van Quyen, J. Martinerie, C. Adam, F. J. Varela, Nonlinear analyses of interictal EEG map the brain interdependences in human focal epilepsy. *Physica D* **127**, 250 (1999). doi:10.1016/S0167-2789(98)00258-9

43. D. Ruelle, *Turbulence, Strange Attractors, and Chaos* (World Scientific, Singapore, 1995).

44. G. F. Gause, *The Struggle for Existence* (Hafner, New York, 1934).

45. L. S. Luckinbill, Coexistence in laboratory populations of *Paramecium aurelia* and its predator *Didinium nasutum*. *Ecology* **54**, 1320 (1973). doi:10.2307/1934194

46. C. Jost, S. P. Ellner, Testing for predator dependence in predator-prey dynamics: A non-parametric approach. *Proc. Biol. Sci.* **267**, 1611 (2000). doi:10.1098/rspb.2000.1186 Medline

47. G. Sugihara, W. Allan, D. Sobel, K. D. Allan, Nonlinear control of heart rate variability in human infants. *Proc. Natl. Acad. Sci. U.S.A.* **93**, 2608 (1996). doi:10.1073/pnas.93.6.2608 Medline

48. C. H. Hsieh *et al*., A comparison of long-term trends and variability in populations of larvae of exploited and unexploited fishes in the Southern California region: A community approach. *Prog. Oceanogr.* **67**, 160 (2005). doi:10.1016/j.pocean.2005.05.002

49. C. H. Hsieh *et al*., Fishing elevates variability in the abundance of exploited species. *Nature* **443**, 859 (2006). doi:10.1038/nature05232 Medline

50. N. C. H. Lo, Egg production of the central stock of northern anchovy, *Engraulis mordax*, 1951-82. *Fish Bull.* **83**, 137 (1985).

51. J. Arnhold, P. Grassberger, K. Lehnertz, C. E. Elger, A robust method for detecting interdependences: Application to intracranially recorded EEG. *Physica D* **134**, 419 (1999). doi:10.1016/S0167-2789(99)00140-2

52. D. Marinazzo, M. Pellicoro, S. Stramaglia, Kernel method for nonlinear Granger causality. *Phys. Rev. Lett.* **100**, 144103 (2008). doi:10.1103/PhysRevLett.100.144103 Medline

53. G. Sugihara, Nonlinear forecasting for the classification of natural time series. *Philos. Trans. R. Soc. London Ser. A* **348**, 477 (1994). doi:10.1098/rsta.1994.0106

54. W. Ebisuzaki, A method to estimate the statistical significance of a correlation when the data are serially correlated. *J. Clim.* **10**, 2147 (1997). doi:10.1175/1520-0442(1997)010<2147:AMTETS>2.0.CO;2

55. C. Hiemstra, J. D. Jones, Testing for linear and nonlinear Granger causality in the stock price-volume relation. *J. Finance* **49**, 1639 (1994).

56. C. Torrence, G. P. Compo, A practical guide to wavelet analysis. *Bull. Am. Meteorol. Soc.* **79**, 61 (1998). doi:10.1175/1520-0477(1998)079<0061:APGTWA>2.0.CO;2

57. M. Detto *et al*., Causality and persistence in ecological systems: A nonparametric spectral granger causality approach. *Am. Nat.* **179**, 524 (2012). doi:10.1086/664628 Medline

58. D. Kugiumtzis, Test your surrogate data before you test for nonlinearity. *Phys. Rev. E* **60**, 2808 (1999). doi:10.1103/PhysRevE.60.2808 Medline

59. H. G. Moser *et al*., *Distributional Atlas of Fish Larvae in the California Current Region: Taxa with Less Than 1000 Total Larvae, 1951 Through 1984* (California Cooperative Oceanic Fisheries Investigations Atlas 32, Scripps Institution of Oceanography, La Jolla, CA, 1994).

60. R. F. Engle, C. W. J. Granger, Co-integration and error correction: Representation, estimation, and testing. *Econometrica* **55**, 251 (1987). doi:10.2307/1913236

61. E. Baek, W. A. Brock, *A General Test for Nonlinear Granger Causality: Bivariate Model* (working paper, Iowa State University and University of Wisconsin, Madison, 1992).

62. T. Schreiber, Measuring information transfer. *Phys. Rev. Lett.* **85**, 461 (2000). doi:10.1103/PhysRevLett.85.461 Medline

63. M. Paluš, A. Stefanovska, Direction of coupling from phases of interacting oscillators: An information-theoretic approach. *Phys. Rev. E* **67**, 055201 (2003). doi:10.1103/PhysRevE.67.055201 Medline

64. Y. Chen, G. Rangarajan, J. Feng, M. Ding, Analyzing multiple nonlinear time series with extended Granger causality. *Phys. Lett. A* **324**, 26 (2004). doi:10.1016/j.physleta.2004.02.032

65. M. E. Pfieger, R. E. Greenblatt, Using conditional mutual information to approximate causality for multivariate physiological time series. *Int. J. Bioelectromagnet.* **7**, 285 (2005).

66. M. Lungarella, K. Ishiguro, Y. Kuniyoshi, N. Otsu, Methods for quantifying the causal structure of bivariate time series. *Int. J. Bifurcat. Chaos* **17**, 903 (2007). doi:10.1142/S0218127407017628

67. K. Hlavackova-Schindler, M. Palus, M. Vejmelka, J. Bhattacharya, Causality detection based on information-theoretic approaches in time series analysis. *Phys. Rep.* **441**, 1 (2007). doi:10.1016/j.physrep.2006.12.004

68. M. Paluš, M. Vejmelka, Directionality of coupling from bivariate time series: How to avoid false causalities and missed connections. *Phys. Rev. E* **75**, 056211 (2007). doi:10.1103/PhysRevE.75.056211 Medline

69. M. Paluš, From nonlinearity to causality: Statistical testing and inference of physical mechanisms underlying complex dynamics. *Contemp. Phys.* **75**, **48**, 307 (2007).

70. L. Faes, G. Nollo, A. Porta, Information-based detection of nonlinear Granger causality in multivariate processes via a nonuniform embedding technique. *Phys. Rev. E* **83**, 051112 (2011). doi:10.1103/PhysRevE.83.051112 Medline

71. J. Geweke, Measurement of linear dependence and feedback between multiple time series. *J. Am. Stat. Assoc.* **77**, 304 (1982). doi:10.1080/01621459.1982.10477803

72. M. Ding, Y. Chen, S. L. Bressler, in *Handbook of Time Series Analysis* (Wiley-VCH, Weinheim, Germany, 2006), pp. 437–460.

73. M. Dhamala, G. Rangarajan, M. Ding, Estimating Granger causality from Fourier and wavelet transforms of time series data. *Phys. Rev. Lett.* **100**, 018701 (2008). doi:10.1103/PhysRevLett.100.018701 Medline

74. C. A. Sims, Macroeconomics and reality. *Econometrica* **48**, 1 (1980). doi:10.2307/1912017

75. S. Johansen, Identifying restrictions of linear equations with applications to simultaneous equations and cointegration. *J. Econom.* **69**, 111 (1995). doi:10.1016/0304-4076(94)01664-L

76. S. Johansen, K. Juselius, Maximum likelihood estimation and inference on cointegration—with applications to the demand for money. *Oxf. Bull. Econ. Stat.* **52**, 169 (1990). doi:10.1111/j.1468-0084.1990.mp52002003.x